

Functional neuroimaging in child psychiatry

Edited by

Monique Ernst

Brain Imaging Center,
National Institute on Drug Abuse, Baltimore, MD, USA

and

Judith M. Rumsey

Clinical Neuroscience Branch,
National Institute of Mental Health, Rockville, MD, USA

With a Foreword by

Joseph T. Coyle

Chairman, Department of Psychiatry, Harvard Medical School, Boston, MA, USA



CAMBRIDGE
UNIVERSITY PRESS

PUBLISHED BY THE PRESS SYNDICATE OF THE UNIVERSITY OF CAMBRIDGE
The Pitt Building, Trumpington Street, Cambridge, United Kingdom

CAMBRIDGE UNIVERSITY PRESS
The Edinburgh Building, Cambridge CB2 2RU, UK
40 West 20th Street, New York, NY 10011-4211, USA
10 Stamford Road, Oakleigh, VIC 3166, Australia
Ruiz de Alarcón 13, 28014 Madrid, Spain
Dock House, The Waterfront, Cape Town 8001, South Africa

<http://www.cambridge.org>

© Cambridge University Press 2000

This book is in copyright. Subject to statutory exception
and to the provisions of relevant collective licensing agreements,
no reproduction of any part may take place without
the written permission of Cambridge University Press.

First published 2000

Printed in the United Kingdom at the University Press, Cambridge

Typeface Utopia 8.5/12 pt. *System* QuarkXPress® [SE]

A catalogue record for this book is available from the British Library

Library of Congress Cataloguing in Publication data

Functional neuroimaging in child psychiatry / edited by Monique Ernst and Judith M. Rumsey
p. ; cm.

Includes index.

ISBN 0 521 65044 5 (hb)

1. Pediatric neuropsychiatry. 2. Brain-Imaging. 3. Developmental neurophysiology.

I. Ernst, Monique, 1953- . II. Rumsey, Judith M.

[DNLM: 1. Mental Disorders - diagnosis - Child. 2. Brain Diseases - diagnosis - Child.

3. Diagnostic Imaging - Child. WS 350 F979 2000]

RJ486.5.F865 2000

618.92'890754-dc 21 99-04455

ISBN 0 521 65044 5 hardback

Every effort has been made in preparing this book to provide accurate and up-to-date information which is in accord with accepted standards and practice at the time of publication. Nevertheless, the authors, editors and publisher can make no warranties that the information contained herein is totally free from error, not least because clinical standards are constantly changing through research and regulation. The authors, editors and publisher therefore disclaim all liability for direct or consequential damages resulting from the use of material contained in this book. Readers are strongly advised to pay careful attention to information provided by the manufacturer of any drugs or equipment that they plan to use.

The views stated herein do not necessarily represent the official views of the National Institute on Drug Abuse, the National Institute of Mental Health, the National Institutes of Health nor the Department of Health and Human Services, nor any other agency of the United States government.

Contents

<i>List of contributors</i>	page vii
<i>Preface</i>	xi
<i>Foreword</i>	xiii
Joseph T. Coyle	

Part 1 Techniques of functional imaging

1 Functional brain imaging with PET and SPECT	3
Peter Herscovitch and Monique Ernst	
2 Modeling of receptor images in PET and SPECT	27
Evan D. Morris, Raymond F. Muzic Jr, Bradley C. Christian, Christopher J. Endres and Ronald E. Fisher	
3 Functional magnetic resonance imaging	45
Guinevere F. Eden and Thomas A. Zeffiro	
4 MRS in childhood psychiatric disorders	59
Deborah A. Yurgelun-Todd and Perry F. Renshaw	
5 Magnetoencephalography	77
Donald C. Rojas, Peter D. Teale and Martin L. Reite	

Part 2 Ethical foundations

6 Ethical issues in neuroimaging research with children	99
L. Eugene Arnold, Alan J. Zametkin, Lauren Caravella and Nicole Korbly	

Part 3 Normal development

7 Brain development and evolution	113
Manuel F. Casanova, Daniel Buxhoeveden and Gurkirpal S. Sohal	

8 Cognitive development from a neuropsychologic perspective	137	17 Eating disorders	298
Daisy M. Pascualvaca and Gloria Morote		Uttom Chowdhury, Isky Gordon and Bryan Lask	
9 Cognitive and behavioral probes of developmental landmarks for use in functional neuroimaging	155		
B. J. Casey, Kathleen M. Thomas, Tomihisa F. Welsh, Rona Livnat and Clayton H. Eccard			
Part 4 Psychiatric disorders		Part 5 Future directions	
<hr/>		<hr/>	
10 Autism	171	18 Techniques of molecular genetics	315
Diane C. Chugani		David J. Vandenberg	
11 Functional imaging in childhood-onset schizophrenia	189	19 Issues in the genetic study of complex neurobehavioral conditions	328
Leslie K. Jacobsen and Alessandro Bertolino		David L. Pauls	
12 Pediatric mood disorders and neuroimaging	205	20 The duplicity of plasticity: a conceptual approach to the study of early lesions and developmental disorders	335
Robert A. Kowatch, Pablo A. Davanzo and Graham J. Emslie		Ralph-Axel Müller and Eric Courchesne	
13 Neuroimaging of childhood-onset anxiety disorders	224	21 Utility of CANTAB in functional neuroimaging	366
David R. Rosenberg, Lori Anne D. Paulson, Frank P. MacMaster and Gregory J. Moore		Andy C. H. Lee, Adrian M. Owen, Robert D. Rogers, Barbara J. Sahakian and Trevor W. Robbins	
14 Tourette's syndrome: what are we really imaging?	242	22 Neurodevelopmental assessment of cognitive function using CANTAB: validation and future goals	379
Bradley S. Peterson and Prakash Thomas		Monica Luciana and Charles A. Nelson	
15 Dyslexia: conceptual issues and psychiatric comorbidity	266	23 Functional neuroimaging in child psychiatry: future directions	398
Frank B. Wood and D. Lynn Flowers		Monique Ernst and Judith M. Rumsey	
16 Attention-deficit hyperactivity disorder: neuroimaging and behavioral/cognitive probes	278		
Julie B. Schweitzer, Carl Anderson and Monique Ernst		<i>Glossary</i>	408
		<i>Index</i>	418
		<i>Colour plates between pp. 82 and pp. 83 and between pp. 242 and pp. 243</i>	

Functional brain imaging with PET and SPECT

Peter Herscovitch and Monique Ernst

Introduction

Functional brain imaging refers to the use of techniques to obtain images of the brain that are related to its physiology or biochemistry, rather than its structural anatomy. Two nuclear medicine-based approaches to functional brain imaging can be used to study the pediatric population, positron emission tomography (PET) and single-photon emission computed tomography (SPECT). Both will be reviewed in this chapter.

PET is a nuclear medicine technique for performing physiologic measurements in vivo. The PET scanner provides tomographic images of the distribution of positron-emitting radiopharmaceuticals in the body. From these images, measurements such as regional cerebral blood flow (rCBF) and glucose metabolism can be obtained. PET has been widely used as a research tool to study normal brain function and the pathophysiology of neurologic and psychiatric disease in adults (Grafton and Mazziotta, 1992; Volkow and Fowler, 1992). Its role in the management of patients with brain disorders is at an earlier stage (Powers et al., 1991) and its use in children has been limited. Conceptually, PET consists of three components: (i) tracer compounds labeled with radioactive atoms that emit positrons; (ii) scanners that provide tomographic images of the concentration of positron-emitting radioactivity in the body; and (iii) mathematical models that describe the in vivo behavior of radiotracers and allow the physiologic process under study to be quantified from the images. The first tomographs for quantitative PET imaging were developed in the mid-1970s (Ter-Pogossian, 1992). Subsequently, instrument design has become more sophisticated, with improved spatial resolution and sensitivity. Radiotracer techniques have been developed to study regional CBF and blood volume; glucose, oxygen, and protein metabolism; blood-brain barrier permeability; numerous neuroreceptor-neurotransmitter

systems; tissue pH; and the concentration of radiolabeled drugs in brain.

SPECT is another nuclear medicine technique that provides tomographic images of radioactivity (George et al., 1991; Wyper, 1993; Green, 1996). SPECT is simpler than PET because it uses radiopharmaceuticals labeled with conventional radionuclides such as technetium-99m (^{99m}Tc); however, it still has the same three components: radiotracers, scanners, and mathematical models. Its quantitative accuracy is less than that of PET and the range of radiopharmaceuticals for studying the brain is relatively limited; it has primarily been used to map cerebral perfusion. Improvements in instrumentation and radiopharmaceuticals are being actively pursued, especially in the development of radiotracers labeled with iodine-123 (^{123}I) to image neuroreceptors (Holman and Devous, 1992; Juni, 1994), and there is a strong interest in clinical SPECT brain studies.

This chapter will provide an overview of PET instrumentation, radiotracers, and mathematical modeling, emphasizing methods to measure cerebral hemodynamics and metabolism, and the most common applications. In addition, SPECT instrumentation and radiopharmaceuticals are described. The analysis and interpretation of functional brain images and special considerations for the pediatric age group are discussed. Methods for studying neurotransmitter systems are treated elsewhere in this volume (Chapter 2). An abbreviated lexicon of various terms used in nuclear medicine is provided in the glossary (p. 408).

Positron emission tomography

Imaging

PET provides tomographic images of the distribution of positron-emitting radioactivity using rings of radiation

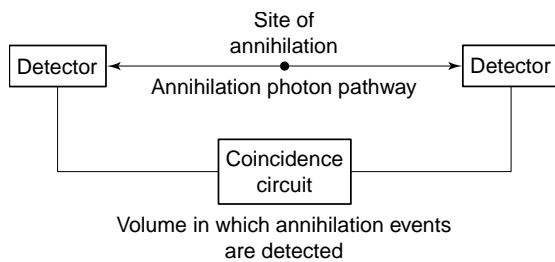


Fig. 1.1. The two high-energy photons resulting from a positron emission and annihilation are detected by two radiation detectors that are connected by an electronic coincidence circuit. A decay event is recorded as a coincidence line between the detectors only when both photons are detected almost simultaneously. A very short time window for photon arrival, typically 5–20 ns, called the coincidence resolving time, is allowed for registration of a coincidence event. This coincidence requirement localizes the site of the annihilation to the volume of space between the detectors.

detectors that are arrayed around the body (or head). Because of the special nature of the positron and the techniques used for image reconstruction, it is possible to obtain absolute radioactivity measurements from these images (Daube-Witherspoon and Herscovitch, 1996).

Formation of the PET image

Certain radioactive atoms, such as oxygen-15 (^{15}O) or fluorine-18 (^{18}F), decay by the emission of a positron from the nucleus. Positrons are the “antimatter” particles to electrons; they have the same mass as electrons but are positively charged. After emission from the nucleus, positrons travel a variable distance in tissue, up to a few millimeters, losing kinetic energy. When almost at rest, they interact with atomic electrons, resulting in the “annihilation” of both particles. Their combined mass is converted into two high-energy (511 keV each) photons that travel in opposite directions from the annihilation site at the speed of light. Detection of these photon pairs is used to measure both the location and the amount of radioactivity in the field of view of the scanner. The two annihilation photons are detected by two opposing radiation detectors connected by an electronic coincidence circuit (Fig. 1.1). This circuit records a decay event only when both detectors sense the almost simultaneous arrival of both photons (the time window for coincidence detection is typically 5–20 ns). The site of the decay event is, therefore, localized to the volume of space between the two detectors, although there is no information about the depth or location of the radioactive source within the volume between the two detectors.

In practice, several rings, each consisting of many radiation detectors, are used. Opposing detector pairs in each

ring are connected by coincidence circuits. With each decay event, the two resulting annihilation photons are detected as a coincidence line; as a result, the number of coincidence lines sensed by any detector pair is proportional to the amount of radioactivity between them. A computer records the coincidence events from each ring. Tomographic images of the underlying distribution of radioactivity are then reconstructed with the same mathematical technique, referred to as filtered back-projection, that is used in conventional X-ray computed tomography (CT) (Hoffman and Phelps, 1986). In addition to filtered back-projection, there are other approaches to image reconstruction. These require considerably more computational time and are used much less frequently.

The intensity of each point or pixel in the reconstructed PET image is proportional to the concentration of radioactivity at the corresponding location in the brain. For the calibration of the scanner to obtain *absolute* radioactivity measurements, a cylinder filled with a uniform solution of radioactivity is imaged. The radioactivity concentration of the solution is then measured with a calibrated well counter, and the scanner calibration factor is calculated to convert PET image counts (in units of cts/s per pixel) to units of radioactivity concentration (e.g., nCi/ml).

Limitations in image quality and quantification

A variety of physical effects, such as attenuation, deadtime losses, scatter, and random coincidences, affect the PET image and are corrected for as part of the image reconstruction process. Other factors such as image noise and spatial resolution also affect image quality and are important considerations in the design and interpretation of PET studies (Hoffman and Phelps, 1986; Karp et al., 1991; Daube-Witherspoon and Herscovitch, 1996).

Attenuation correction

A key step in image reconstruction is correction for the absorption or attenuation of annihilation photons that occurs through their interactions with tissue (Bailey, 1998). This substantially decreases the number of coincidence counts detected. Although the amount of attenuation can be estimated using an assumed value for the attenuating properties of tissue, actual measurements are more accurate. Before the administration of the radiotracer, a separate “transmission scan” is performed with a source of positron-emitting radioactivity positioned between the subject’s head and the detector rings. The outside source, filled with germanium-68/gallium-68 ($^{68}\text{Ge}/^{68}\text{Ga}$) radioactivity, is a ring or a rod that is rotated around the body. A similar measurement is made with nothing in the scanner field of view. The ratio of the two measurements gives the amount

of attenuation between each detector pair and is used in the image reconstruction process to correct for attenuation.

To respond to the demands of some protocols in which there is a long delay between radiotracer administration and subsequent emission scanning, techniques have been devised to calculate the attenuation correction using a transmission scan obtained *after* radiotracer administration, that is, with positron-emitting radioactivity still in the body (Carson et al., 1988). This approach is particularly useful when using (^{18}F)-labeled deoxyglucose (FDG) to measure regional cerebral glucose metabolism (rCMRGlucose; see below).

Image noise

The PET image has inherent statistical noise because of the random nature of radioactive decay. The disintegration rate of a radioactive sample undergoes moment-to-moment variation. The resultant uncertainty in measuring the amount of radioactivity decreases as the number of counts recorded increases. Similarly, the statistical reliability of a PET measurement depends on the number of counts. The situation is more complex, however, because the value of radioactivity in any small brain region is obtained from an image reconstructed from multiple views or projections of the radioactivity distribution throughout the entire brain slice. Therefore, the noise in any individual brain region is affected by noise in other brain regions and tends to be greater (Budinger et al., 1978). Excessive noise gives the PET image a grainy, "salt and pepper" appearance and decreases the ability to quantitate radioactivity accurately.

Image noise depends upon the number of counts collected, which in turn depends upon scanner sensitivity, the duration of the scan, and the concentration of radioactivity in the field of view. Scanner sensitivity (measured in units of (counts/s)/($\mu\text{Ci/ml}$)), is determined by its design features, such as the nature and arrangement of the radiation detectors. For example, the sensitivity is inversely proportional to the diameter of the detector rings. Although increasing scan duration increases counts, this is frequently not possible, either because of the short half-life of the radiotracer or because it would not be compatible with the tracer-kinetic mathematical model that is used. Administering more radioactivity increases counts, but this approach is limited by radiation safety considerations and also by the inability of tomographs to operate accurately at high count rates, that is by count rate performance.

Deadtime losses and random coincidences

Count rate performance refers to the level of radioactivity that can be accurately measured with a PET scanner. It is limited by deadtime loss and by random coincidences.

Deadtime loss is the decreasing ability of a scanner to register counts as the count rate increases because of the time required by the physical processes involved in handling each count. Deadtime loss originates from limitations of the electronic circuitry used to process information from the detectors and from the recovery time of the detectors themselves. Deadtime causes a reduction in measured coincidences as radioactivity increases in the field of view of the scanner. This reduction can be predicted for a given count rate and a correction factor can be applied. This correction, no matter how accurate, does not compensate for the loss in statistical accuracy of the image that occurs because fewer counts were actually collected.

Random coincidences also limit count rate performance. These occur when two photons from two *different* positron annihilations are sensed by a detector pair within the coincidence resolving time; as a result, a false or random coincidence count is collected. The fraction of total coincidences recorded that are random increases linearly with radioactivity. Random coincidences add noisy background to the image. Although corrections can be made that subtract an estimate of these false counts, the contribution to the image noise persists (Hoffman et al., 1981). Therefore, for any given tomograph, the amount of radioactivity administered must be carefully selected to balance the competing effects of improved counting statistics with the "diminishing returns" resulting from deadtime and random coincidences.

Scatter

Another source of background noise in the PET image is scatter. Scatter occurs when an annihilation photon traveling in tissue is deflected in a collision with an electron and its direction changes. This results in incorrect positioning of the coincidence line. Not only is information lost from the affected coincidence line but also a noisy background level is added to the image. This leads to an overestimation of radioactivity, especially in areas containing relatively less radioactivity, e.g., regions with low blood flow or metabolism. The amount of scatter in an image is a function of the distribution of radioactivity, the anatomy of the tissue scattering the photons, and the design of the scanner. It is necessary to correct for scatter because it can contribute up to 20% of the counts in an image. Methods have been developed to correct for scatter that vary in their complexity and effectiveness (Bergstrom et al., 1983; Hoffman and Phelps, 1986).

Spatial resolution

A critical issue in interpreting PET (and SPECT) images is the concept of image resolution. Image resolution is the

minimum distance by which two points of radioactivity must be separated to be perceived independently in the reconstructed image. Limited resolution, which is visually apparent as blurring of the image, has a major effect on the ability to quantify radioactivity accurately, especially in small structures (see below).

In PET, image resolution depends upon the accurate localization of positron-emitting nuclei. This is limited by the physics of positron annihilation and by detector design. Annihilation photons are produced only after the positron has traveled up to several millimeters from the nucleus. This limits the accuracy of localizing the nucleus. The distance the positron travels (positron range) varies and depends on the specific radionuclide and tissue density; it averages 1.2 mm for ^{18}F , 2.1 mm for ^{11}C . In addition, the angle between the two annihilation photons deviates slightly from 180° , causing a slight misplacement of the coincidence line (noncolinearity of the annihilation photons). These effects result in a 1–3 mm resolution loss (Phelps and Hoffman, 1976) and are larger when the detectors are farther apart, as in a body scanner compared with a head scanner. Detector size and shape determine how accurately the position of each coincidence line is recorded; smaller detectors provide better resolution.

Resolution is measured by imaging a thin line source of positron-emitting radioactivity (Fig. 1.2). Because of limited resolution, the radioactivity in the source appears blurred or spread out over a large area; resolution is defined by the amount of spreading. The resolution of current scanners is about 4–5 mm in the image plane (de Grado et al., 1994; Wienhard et al., 1994).

PET Instrumentation

A PET system consists of many components (Hoffman and Phelps, 1986; Council on Scientific Affairs, 1988; Koeppe and Hutchins, 1992). Several rings of radiation detectors are mounted in a gantry. Each detector consists of a small scintillation crystal that gives off light when the energy of an annihilation photon is deposited in it. The detector is coupled to a photomultiplier tube that converts the light pulse to an electrical signal which is fed into the coincidence circuitry. Scanners have numerous rings, each containing up to several hundred detectors (de Grado et al., 1994; Wienhard et al., 1994), with a tomographic slice provided by each ring. In addition, "cross-slices" halfway between the detector rings are derived from coincidences between detectors in adjacent rings. Therefore, 47 contiguous slices can be obtained simultaneously by a 24-ring system. To date, the most sophisticated scanners have 32 rings, which permit the acquisition of 63 slices. A dedicated computer is used to control the scanning process, collect

the coincidence count information, and reconstruct and display the images.

During the scan, the subject lies on a special table that is fitted with a head holder to restrain head movement. The gantry has low-powered lasers that project lines onto the subject's head and aid in positioning. Some gantries can be tilted from the vertical to obtain slices in specific planes, for example parallel to the canthomeatal line.

A relatively recent, major advance in scanner design permits coincidence counts to be collected by opposing detectors that do not have to be in the same or adjacent rings (Spinks et al., 1992; de Grado et al., 1994; Bailey et al., 1998). Because more coincidence lines are collected by this three-dimensional (3D) imaging approach, scanner sensitivity is substantially increased. This improves image quality or, alternatively, permits the same number of image counts to be obtained with less administered radioactivity. These factors are a great benefit in pediatric imaging, in which radiation exposure is a particular consideration. The disadvantages of 3D acquisition are an increase in the amount of scatter and contribution from radioactivity outside the field of view (i.e., from other parts of the body) to the counts seen by the detector rings. This can be more of a problem when scanning small pediatric subjects because the rest of the body is closer to the gantry than it is in adults.

Positron-emitting radiotracers

The second requirement for PET is a radiotracer of physiologic interest that is labeled with a positron-emitting radionuclide. A radiotracer can be a naturally occurring compound in which one of the atoms is replaced with its radioactive counterpart or it can be a labeled analog which behaves *in vivo* similarly to the natural substance. It can also be a synthetic substance, such as a radiolabeled drug, that interacts with a specific biologic system.

The positron-emitting nuclides most commonly used to label PET radiotracers are ^{15}O , ^{13}N , ^{11}C , and ^{18}F with half-lives of 2.05, 10.0, 20.3, and 109.8 min, respectively. (The half-life is the time required for radioactivity to decay to one-half of its original value.) The chemical nature of ^{15}O , ^{13}N , and ^{11}C is identical to that of their non-radioactive counterparts, which are basic constituents of living matter as well as of most drugs. Consequently, they can be incorporated into radiotracers with the same *in vivo* behavior as the corresponding nonradioactive compound. Fluorine-18 is used to substitute for hydrogen or hydroxyl groups to synthesize analogs with characteristics similar to those of the unsubstituted compound. Drugs that would normally contain fluorine can be synthesized as their ^{18}F -labeled counterparts. Relatively large

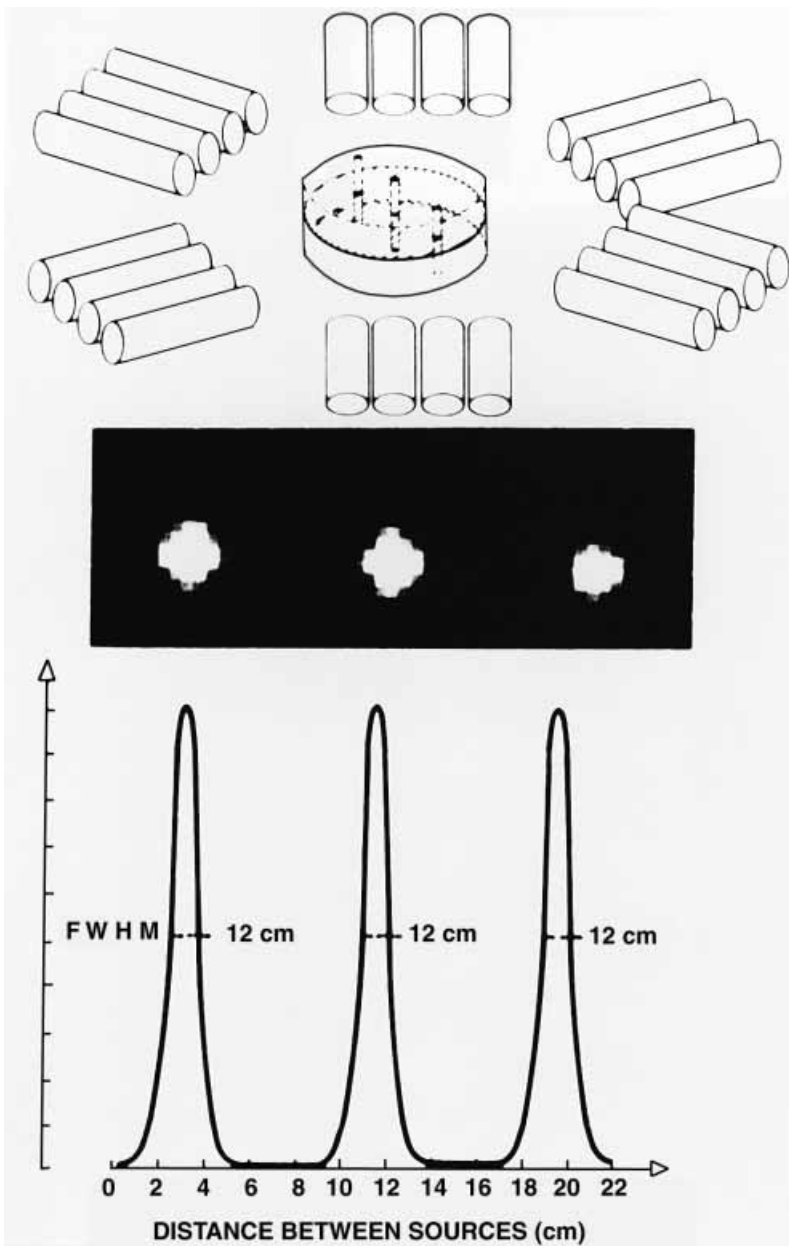


Fig. 1.2. Definition and measurement of the resolution of a PET scanner. Thin line sources of positron-emitting radioactivity perpendicular to the image plane are scanned (upper panel). Because of resolution limitations, the radioactivity in each source appears blurred or spread over a larger area (middle panel). Scanner resolution is defined by the amount of spreading that occurs. A plot of the image intensity along a line through the center of the images (lower panel) shows that this spreading approximates a bell-shaped or Gaussian curve. The width of this curve at one-half of its maximum height (termed the full width at half maximum, FWHM) is the measure of resolution. Here the resolution is 1.2 cm. Another interpretation of the FWHM is that it is the minimum distance by which two points of radioactivity must be separated to be independently perceived in the reconstructed image. (From Ter-Pogossian et al. 1975, with permission.)

Table 1.1. Representative PET radiotracers

Physiologic process or system	Radiotracer
<i>Cerebral blood flow</i>	H ₂ ¹⁵ O [¹⁵ O]-Butanol; [¹¹ C]-butanol, [¹⁸ F]-fluoromethane
<i>Cerebral blood volume</i>	C ¹⁵ O; ¹¹ CO
<i>Cerebral energy metabolism</i>	
Oxygen metabolism	¹⁵ O ₂
Glucose metabolism	[¹⁸ F]-Fluorodeoxyglucose; [¹¹ C]-deoxyglucose, [¹¹ C]-glucose
Glucose transport	[¹¹ C]-3- <i>O</i> -Methylglucose
<i>Neuroreceptor systems</i>	
Dopaminergic	
Presynaptic dopamine pool	[¹⁸ F]-Fluoro- <i>L</i> -dopa; [¹⁸ F]-fluoro- <i>L</i> - <i>m</i> -tyrosine
Dopamine D ₂ receptors	[¹¹ C]- <i>N</i> -Methylspiperone; [¹¹ C]-raclopride; [¹⁸ F]-spiperone; [¹⁸ F]- <i>N</i> -methylspiperone
Dopamine D ₁ receptors	[¹¹ C]-SCH23390
Dopamine reuptake sites	[¹¹ C]-Nomifensine; [¹¹ C]-cocaine; [¹⁸ F]-labeled 1-[2-(diphenylmethoxy)ethyl]-4-(3-phenyl-2-propenyl)piperazine ([¹⁸ F]-GBR)
Opiate	[¹¹ C]-Carfentanil; [¹¹ C]-diprenorphine, [¹⁸ F]-cyclofoxy
Benzodiazepine	[¹¹ C]-Flumazenil
Serotonergic (5-HT)	
Presynaptic serotonin pool	[¹¹ C]- α -Methyltryptophan
5-HT _{1A} receptors	[¹¹ C]-WAY100,635
5-HT _{2A} receptors	[¹¹ C]-MDL100,907; [¹⁸ F]-altanserin; [¹⁸ F]-setoperone
5-HT reuptake sites	[¹¹ C]-McN5652
Monoamine oxidase B	[¹¹ C]-Deprenyl
<i>Amino acid transport, protein synthesis</i>	[¹¹ C]-Methionine; [¹¹ C]-leucine; [¹¹ C]-tyrosine
<i>Tissue pH</i>	¹¹ CO ₂ ; [¹¹ C]-Dimethadione
<i>Tissue drug kinetics</i>	[¹¹ C]-Phenytoin; [¹¹ C]-valproate; [¹³ N]-carmustine (BCNU)

Note: This is a partial listing of radiotracers that have been used to study physiologic processes or systems in the brain with PET. The most commonly used radiotracer methods are those to measure regional cerebral blood flow and metabolism.

amounts of these radionuclides with short half-lives can be administered to provide good-quality images with acceptable radiation exposure because of their rapid decay. The short half-lives, especially of ¹⁵O, permit repeat studies in the same subject in one experimental session because of the rapid physical decay after each administration.

The disadvantage of these short half-lives is that the synthesis of PET radiotracers is demanding. On-site production of radionuclides by means of a cyclotron is required (Wolf and Schlyer, 1993), and rapid techniques must be devised for radiotracer synthesis and quality control. These must yield products that are pure, sterile, and nontoxic. The tracer must have the appropriate properties to permit the desired physiologic measurement to be made (Kilbourn, 1991; Dannals et al., 1993). Important factors include its permeability across the blood-brain

barrier, the formation and fate of any radioactive metabolites, the ability to develop a mathematical model to describe the behavior of the tracer, and, for neuroreceptor ligands, the binding characteristics. Preclinical studies are typically performed, using tissue sampling or autoradiography in small animals and PET studies in large ones. The recent development of PET scanners designed to image small animals (e.g., rat), should facilitate the preclinical assessment of new PET tracers (Cherry et al., 1998). A wide variety of positron-emitting radiopharmaceuticals has been synthesized (Table 1.1) (Fowler and Wolf, 1991).

Radiotracer modeling

A mathematical model is required to calculate the value of the physiologic variable of interest from measurements of

radiotracer concentration in brain and blood. The model describes the *in vivo* behavior of the radiotracer, that is the relationship over time between the amount of tracer delivered to a brain region in its arterial input and the amount of tracer in the region. The use of models allows PET to be a quantitative physiological technique rather than only an imaging modality (Huang and Phelps, 1986; Carson, 1991, 1996). Compartmental models are typically used. It is assumed that there are entities called compartments that have uniform biologic properties and in which the tracer concentration is uniform at any instant in time. The compartments can be physical spaces such as the extravascular space, or biochemical entities such as neuroreceptor-binding sites. The model is described by one or more equations, that contain measurable terms (i.e., the brain and blood radiotracer concentrations over time) and unknowns such as blood flow or receptor concentration that are of interest.

Several factors must be considered in developing a model. These include tracer transport across the blood–brain barrier, the behavior of the tracer in brain, the presence of labeled metabolites in blood, the potential for alterations in tracer behavior if there is pathology, and the ability to solve the model accurately for the unknown parameters. Error analysis and model validation are important. Error analysis consists of mathematical simulations to determine the sensitivity of the model to potential sources of measurement error. Validation experiments are usually performed to demonstrate that the method provides reproducible, accurate, and biologically meaningful measurements.

This chapter will describe the PET methods used to measure rCBF and cerebral blood volume (rCBV) and glucose and oxygen metabolism. Measurements of CBF glucose metabolism are widely used as indices of neuronal activity (see below). In addition, SPECT tracer methods for assessing cerebral perfusion will be discussed.

PET radiotracer techniques

Cerebral glucose metabolism

The measurement of rCMRGlucose utilizes FDG. The approach is based on the technique used to measure rCMRGlucose in laboratory animals with [¹⁴C]-deoxyglucose and tissue autoradiography (Sokoloff et al., 1977) and adapted for PET by using ¹⁸F as the label (Phelps et al., 1979; Reivich et al., 1979; Huang et al., 1980). FDG is a glucose analog in which a hydroxyl group has been replaced with an ¹⁸F atom. FDG is transported across the blood–brain barrier and is phosphorylated in tissue, as is glucose, by hexokinase to form FDG 6-phosphate (FDG-6-P). Because of its anomalous struc-

ture, however, FDG-6-P cannot proceed further along the glucose metabolic pathway. Also, there is little dephosphorylation of FDG-6-P back to FDG. As a result of this “metabolic trapping”, there is negligible loss of FDG-6-P. This facilitates the calculation of rCMRGlucose from measurements of local tissue radioactivity. Sokoloff’s three-compartment model applied to FDG consists of plasma FDG in brain capillaries, free FDG in tissue, and FDG-6-P in tissue (Fig. 1.3*a*). Rate constants describe the movement of tracer between these compartments. An operational equation permits the calculation of rCMRGlucose from the tissue radioactivity concentration, the arterial plasma concentration of FDG over time, and the plasma glucose concentration (Fig. 1.3*b*). The equation also contains the rate constants and a factor termed the lumped constant (LC). The LC corrects for the differences between glucose and FDG in blood–brain barrier transport and in phosphorylation. Neither the rate constants nor the LC can be routinely determined for each experimental subject or condition. It was found possible, however, to use standard values that can be determined once in separate groups of normal subjects.

To implement the method, images are obtained starting 30–45 min after intravenous injection of 5–10 mCi FDG. Blood is sampled to measure the concentrations of glucose and FDG in plasma over time. The operational equation with standard values for the rate constants and LC is used to generate images of rCMRGlucose (Fig. 1.4). Typical normal values of rCMRGlucose are 6–7 and 2.5–3 mg/min per g tissue in gray and white matter, respectively. (Sasaki et al., 1986; Hatazawa et al., 1988; Tyler et al., 1988; Camargo et al., 1992).

Measurements of rCMRGlucose with FDG reflect the state of the subject primarily during the first 10–20 min after tracer injection (Huang et al., 1981). This means that if a challenge is used, such as cognitive, motor, or pharmacologic activation, it must start slightly before FDG injection and continue for some time. If unwanted subject activity occurs during tracer uptake, such as anxiety or fidgeting, it will affect the results particularly if it occurs during the first 10–20 min.

The accuracy of using standard values for the rate constants and LC has been the subject of considerable discussion (Cunningham and Cremer, 1985; Baron et al., 1989). Their values may change in the presence of pathology, and the use of incorrect values results in inaccurate rCMRGlucose calculations (Sokoloff et al., 1977; Sokoloff, 1985). Because the terms in the operational equation containing rate constants approach zero with increasing time (see Fig. 1.3*b*), a delay of 30–45 min between FDG injection and PET imaging is used to minimize the error associated with using standard values. There can still be substantial error

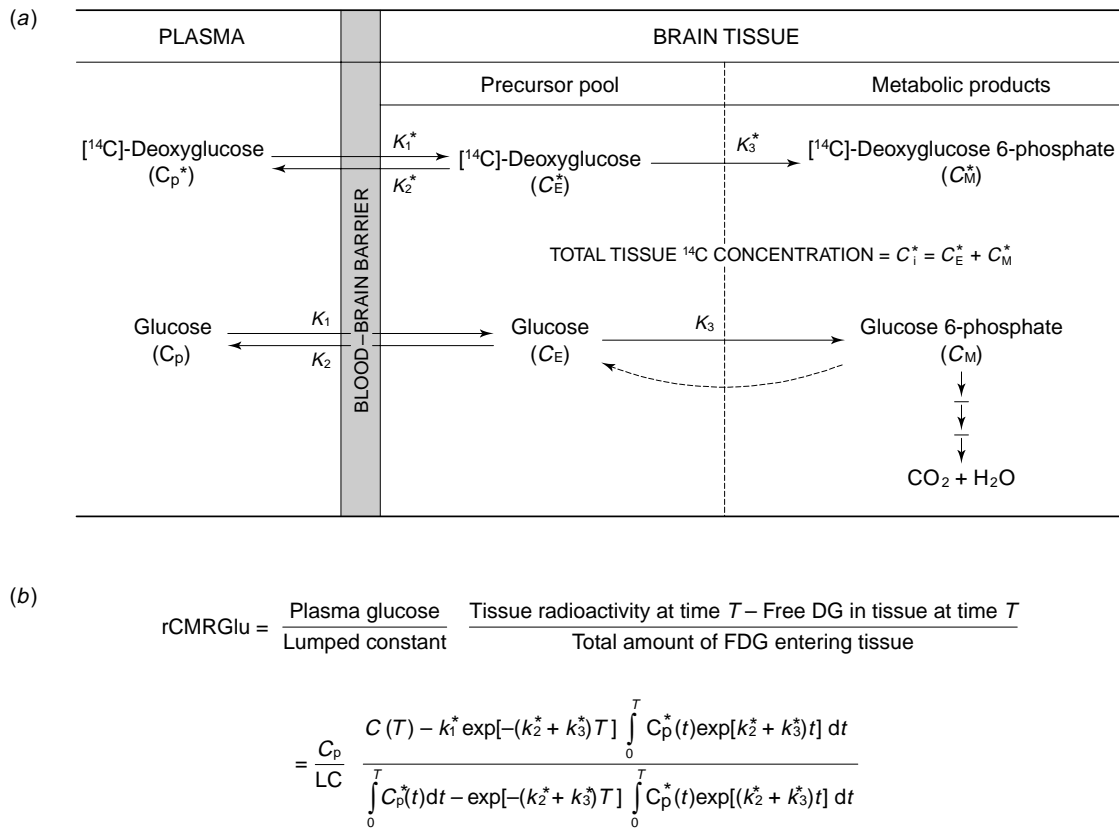


Fig. 1.3. Measurement of regional cerebral glucose metabolism (rCMRGlucose) using deoxyglucose (DG) labeled with ¹⁸F (FDG). (a) The Sokoloff three-compartment model used to measure rCMRGlucose with DG. The compartments consist of DG in the plasma in brain capillaries, DG in brain tissue, and DG 6-phosphate (DG-6-P) in tissue. Rate constants describe the movement of tracer between compartments, two for the bidirectional transport of DG across the blood-brain barrier between plasma and tissue (k_1^* , k_2^*), and one for the phosphorylation of DG to DG-6-P (k_3^*). In the adaptation of this model to PET, FDG is used and a fourth rate constant, k_4^* , is added to account for the small amount of dephosphorylation of FDG-6-P back to FDG. (From Sokoloff, 1977, with permission.) (b) The operational equation of the DG method. The equation in words aids in understanding the model. The terms that are measured are $C(T)$, the tissue radioactivity concentration at time T , typically 30–45 min after DG administration; $C_p^*(t)$, the plasma DG concentration over time; and C_p , the plasma glucose concentration. The concentration of free DG in tissue at time T is calculated from $[C_p^*(t)]$ and the rate constants. The difference between the two terms in the numerator is the concentration of DG-6-P that has been formed. The denominator equals the amount of DG delivered to tissue. Therefore, the ratio on the right-hand side is the fractional rate of phosphorylation of DG. Multiplying this ratio by C_p would give the rate of glucose phosphorylation if DG and glucose had the same behavior. Because this is not the case, the lumped constant (LC) is included to account for the difference. The adaptation of this equation to PET using FDG is more complex because of the inclusion of a fourth rate constant, k_4^* .

in the presence of cerebral ischemia or a tumor, however (Wienhard et al., 1985; Nakai et al., 1987; Graham et al., 1989). Several investigators reformulated the operational equation to decrease its sensitivity to the rate constants and have refined the methods to measure them from sequential PET images (Brooks, 1982; Lammertsma et al., 1987).

The LC is assumed to be uniform and constant throughout brain under normal physiologic conditions, based on theoretical arguments. Originally, the value for the LC in

humans was selected so that the average whole brain CMRGlucose measured with FDG would equal that determined by earlier investigators with the more invasive Kety-Schmidt technique (Phelps et al., 1979). It is possible to measure the LC of whole human brain from the ratio of the brain arteriovenous extraction fraction of FDG to that of glucose (Reivich et al., 1985). A recent study (Hasselbalch et al., 1998) in which great care was taken in the methodologic aspects of the measurement obtained a value for the LC in normal subjects of 0.81, higher than the

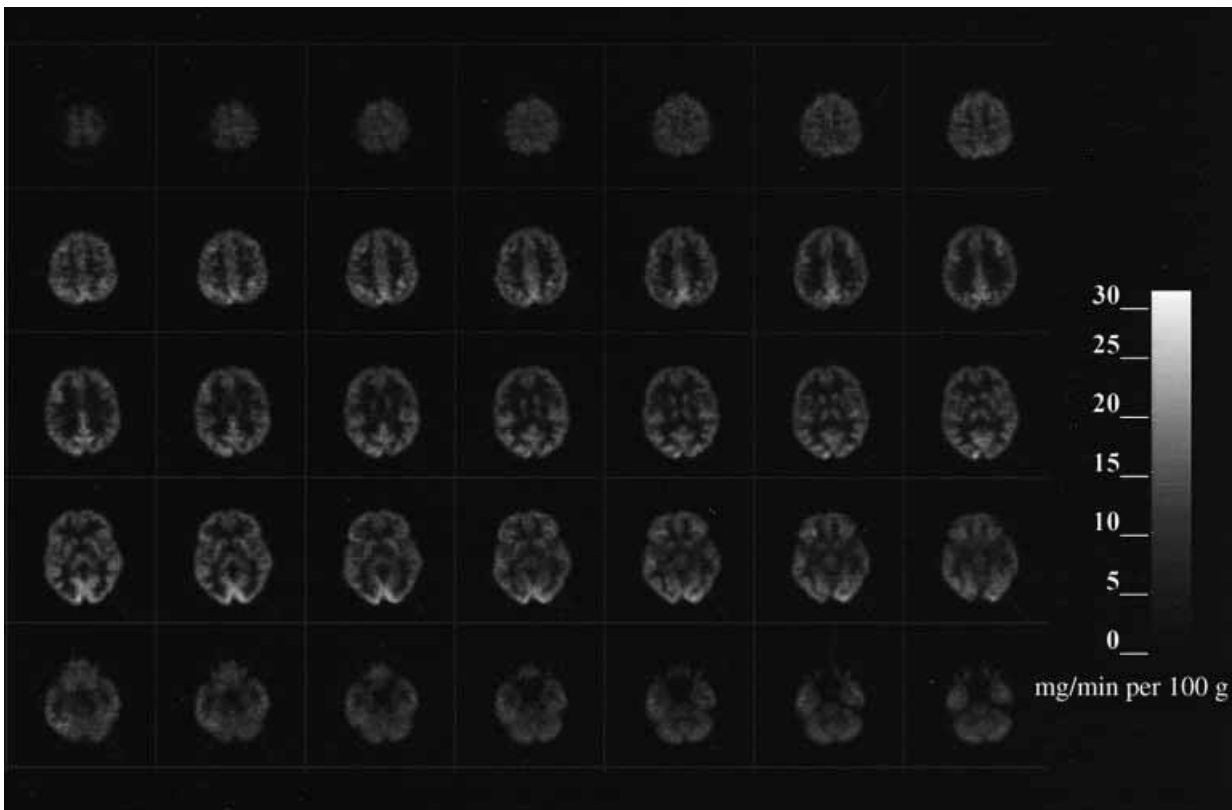


Fig. 1.4. Cerebral glucose metabolic rates. Quantitative images obtained in a normal subject with [^{18}F]-fluorodeoxyglucose and application of Sokoloff's model. Anterior is up and left is to the reader's left. These images start at the level of the superior cortical level (upper left) and proceed down through the brain to the level of the cerebellum. Note the bar scale at the right indicating the correspondence between glucose metabolic rates and gray levels in the image.

values of 0.42–0.52 used in earlier work. The LC does change in pathologic conditions such as acute cerebral ischemia, recent cerebral infarction, and brain tumor (Gjedde et al., 1985; Nakai et al., 1987; Spence et al., 1990; Greenberg et al., 1992). Since calculated rCMRglu is inversely proportional to the LC (see Fig. 1.3), the use of an incorrect value leads to a corresponding error in the calculation. Consequently, it is necessary to redetermine both the LC and the rate constants to avoid such errors in pathologic conditions where there is a gross abnormality of tissue or an imbalance between glucose supply and demand. This is difficult and has been rarely done in PET studies.

An alternative approach to measure rCMRglu uses [^{11}C]-glucose, which is transported and metabolized in the same way as glucose (Blomqvist et al., 1990). As a result, the compartmental model does not require a LC correction factor. A disadvantage is that the labeled metabolites of glucose, such as $^{11}\text{CO}_2$, are not all trapped in tissue and the model must account for their egress. [^{11}C]-Glucose may be

more widely used in the future, especially in pathologic conditions. For example, it has been recently used to measure cerebral glucose transport and metabolism in preterm infants (Powers et al., 1998).

Cerebral blood volume

Measurement of rCBV uses trace amounts of ^{11}CO or C^{15}O administered by inhalation (Grubb et al., 1978; Martin et al., 1987). The tracer binds to hemoglobin and is confined to the intravascular space. Local radioactivity in brain is proportional to its red cell content; consequently, rCBV can be calculated from the ratio of the radioactivity in brain to that in peripheral blood. However, the hematocrit is less in brain than in peripheral large vessels owing to the behavior of blood in the brain microvasculature, and the ratio of cerebral hematocrit to peripheral hematocrit (R) must be incorporated into the calculation (Grubb et al., 1978; Lammertsma et al., 1984; Martin et al., 1987). Equation (1.1), or a modification (Videen et al., 1987), is used to calculate rCBV in units of milliliters per 100g

tissue, from the radiotracer concentrations in tissue (C_t) and blood (C_{bl}):

$$rCBV = \frac{C_t}{C_{bl}R} \quad (1.1)$$

The use of $C^{15}O$ has practical advantages over ^{11}CO (Martin et al., 1987). The 2 min half-life of ^{15}O permits other PET studies to be performed with little delay and lowers radiation exposure, and the synthesis is more convenient. Normal values for rCBV are 4–6 ml/100 g in gray matter and 2–3 ml/100 g in white matter (Lammertsma et al., 1983; Perlmutter et al., 1987).

In cerebrovascular disease, rCBV reflects vasodilatation in response to decreased cerebral perfusion pressure, as may occur with a narrowed internal carotid artery (Powers, 1991; Heiss and Podreka, 1993). Changes in rCBV can also be seen with elevated intracranial pressure (Grubb et al., 1975). In addition, rCBV data may be required as part of other PET methods (e.g., the measurement of cerebral oxygen metabolism and extraction fraction or some neuro-receptor studies) to correct for radiotracer located in the intravascular space so as to determine the amount of radiotracer that actually enters tissue. Measurement of rCBV has recently been used to determine the vascular response to focal brain activation (Wang et al., 1998).

Cerebral blood flow

Methods to measure rCBF with PET are based on a model developed by Kety to measure rCBF in laboratory animals (Kety, 1951; Landau et al., 1955). The model describes inert tracers that can diffuse freely across the blood–brain barrier. The technique involves infusing a radioactive tracer over a brief time period T , often 1 min. Frequent timed blood samples are obtained during the infusion to determine the arterial time–radioactivity curve $C_a(t)$. The animal is then killed. Regional brain radioactivity at the end of the infusion, $C_t(T)$, is measured by quantitative tissue autoradiography. Tissue blood flow f (units of ml/min per 100 g) is calculated from these measurements using Eq. (1.2):

$$C_t(T) = f \int_0^T C_a(t) \exp[-f/\lambda(T-t)] dt \quad (1.2)$$

Where λ is the brain–blood partition coefficient for the tracer defined as the ratio between the tissue and blood radiotracer concentrations when they are in equilibrium. Its value can be determined from independent experiments or can be calculated as the ratio of the solubilities of the tracer in brain and blood (Kety, 1951; Herscovitch and Raichle, 1985). Equation (1.2) is solved numerically for flow, using measured values for $C_t(T)$ and $C_a(t)$, and a specified value for λ .

Kety's method is the basis for methods to measure rCBF with PET. Although there are different approaches, they all involve administering a diffusible, positron-emitting radiotracer, blood sampling to determine the time–activity curve in arterial blood (typically from the radial artery), and the application of a modification of Eq. (1.2) to generate images of rCBF from PET images of radioactivity. The tracer most commonly used is $[^{15}O]$ -water ($H_2^{15}O$) administered by intravenous injection. Because of the short half-life of ^{15}O , repeat measurements can be performed within 10–12 min.

The steady-state method was the earliest widely used PET method to measure rCBF (Subramanyam et al., 1978; Frackowiak et al., 1980). The subject inhales $C^{15}O_2$ delivered at a fixed rate. The action of carbonic anhydrase in red blood cells results in transfer of ^{15}O to water and the $H_2^{15}O$ constantly generated in the lungs circulates throughout the body. A steady state is reached in which radioactivity delivered to brain tissue equals that leaving by decay and by venous washout. The brain distribution of radioactivity remains constant, and a simple equation can be used to calculate rCBF. This method was convenient with the early, single-ring tomographs, since multiple tomographic slices could be obtained by repositioning the patient during $C^{15}O_2$ inhalation. A limitation is the nonlinear relationship between rCBF and tissue radioactivity, which increases the sensitivity of the CBF calculation to errors in measured tissue and blood radioactivity (Lammertsma et al., 1981; Herscovitch and Raichle, 1983; Baron et al., 1989). Because of this, the long period required for CBF measurement, and the development of multislice scanners, the steady-state method has been largely supplanted.

Alternative approaches use bolus intravenous injections of $H_2^{15}O$ and an adaptation of Kety's equation. Equation (1.2) is not used directly because scanners cannot measure the instantaneous brain radiotracer concentration $C_t(T)$. It has been modified in different ways to allow for performance of the scans over many seconds, summing enough counts to obtain satisfactory images. With the PET/autoradiographic approach, $H_2^{15}O$ is administered by bolus intravenous injection, and a 40 s scan is obtained after the radiotracer arrives in the head (Herscovitch et al., 1983; Raichle et al., 1983). The relationship between tissue counts and rCBF is almost linear and errors in measurement of tissue radioactivity result in approximately equivalent errors in calculated rCBF. Because the PET image obtained with a brief scan (1 min or less) closely reflects flow differences in different brain regions, useful information about relative CBF can be obtained without blood sampling. This approach is widely used in functional brain mapping experiments, in which $H_2^{15}O$ images are used to

determine relative rCBF changes during neurobehavioral tasks (Frackowiak and Friston, 1994). Average values for rCBF in normal subjects obtained with either the steady-state method (Leenders et al., 1990) or the PET/autoradiographic method (Herscovitch et al., 1987; Perlmutter et al., 1987) are 40–60 ml/min per 100 g in gray matter and 20–30 ml/min per 100 g in white matter.

There are other methods for measuring rCBF based on the Kety model. One approach involves collecting several sequential, brief images after bolus intravenous administration of tracer (Koeppel et al., 1985). Parameter estimation techniques are used to estimate both rCBF and λ from the scan and blood radioactivity data. To simplify blood sampling for these $H_2^{15}O$ rCBF techniques, automated systems have been designed to withdraw arterial blood continuously past a radiation detector (Eriksson et al., 1988).

Methods using $H_2^{15}O$ assume that it is freely diffusible across the blood–brain barrier. However, there is a modest diffusion limitation, which results in an underestimation of rCBF at higher flows (Raichle et al., 1983). There are other tracers without a diffusion limitation, such as [^{11}C]- or [^{15}O]-butanol (Herscovitch et al., 1987; Berridge et al., 1991). The diffusion limitation of $H_2^{15}O$ is accepted, however, because of the tracer's convenience. Also, in conditions with decreased rCBF, tracer diffusion limitation is less important.

Cerebral oxygen metabolism

The regional cerebral metabolic rate of oxygen (rCMRO₂), which is more complex to obtain than cerebral glucose metabolism, is not widely used in research in pediatric disorders. It is measured using inhaled $^{15}O_2$. One method developed in conjunction with the steady-state rCBF technique uses continuous inhalation of $^{15}O_2$ (Subramanyam et al., 1978; Frackowiak et al., 1980). Another, a companion to the PET/autoradiographic rCBF method, uses a brief inhalation of $^{15}O_2$ (Mintun et al., 1984). The principles underlying these methods are similar. Approximately 35–40% of the oxygen delivered to the brain is extracted and metabolized (Perlmutter et al., 1987; Leenders et al., 1990). Both methods measure this oxygen extraction fraction (OEF). There are essentially no stores of oxygen in brain, and all extracted oxygen is metabolized. Therefore, rCMRO₂ can be determined from the product of OEF and the rate of oxygen delivery to brain, which equals rCBF multiplied by arterial oxygen content. The tracer models describe the fate of the ^{15}O label following $^{15}O_2$ inhalation. Extracted $^{15}O_2$ is metabolized to $H_2^{15}O$, which is then washed out of brain. The $H_2^{15}O$ that is produced by brain as well as by the rest of the body recirculates to brain and

diffuses into and out of brain tissue. Another component of the measured radioactivity is intravascular $^{15}O_2$ that is not extracted by brain. It is necessary to account for this component so that it is not attributed to radioactivity in tissue. Therefore, an independent measurement of rCBV is needed. Both PET methods require three scans to measure regional oxygen extraction fraction (rOEF) and rCMRO₂: an rCBF scan, an rCBV scan, and a scan obtained with $^{15}O_2$.

With the steady-state method, scanning is performed during continuous inhalation of $^{15}O_2$ and rCBF is measured with continuous inhalation of $C^{15}O_2$ and rCBV with $C^{15}O$. The rOEF is computed from these scans and from measurements of blood radioactivity (Lammertsma et al., 1983). An alternative method for measuring rOEF and rCMRO₂ uses a brief inhalation of $^{15}O_2$ (Mintun et al., 1984; Videen et al., 1987). A 40 s scan is obtained following $^{15}O_2$ inhalation, and frequent arterial blood samples are collected for measurements of blood radioactivity. It also involves measurement of rCBF with $H_2^{15}O$ and the PET/autoradiographic method, and of rCBV with $C^{15}O$. The method was validated in baboons in a series of experiments that included very reduced rCMRO₂ (Mintun et al., 1984; Altman et al., 1991). A different approach has been described to measure rCMRO₂ that involves dynamic scanning (i.e., obtaining multiple short scans over time) following only one brief inhalation of $^{15}O_2$ (Ohta et al., 1992). Average normal values for gray matter rCMRO₂ are 2.5–3.5 ml/min per 100 g (Perlmutter et al., 1987; Leenders et al., 1990).

Single photon emission computed tomography

Principles

The radionuclides used in SPECT decay by emitting a single photon or gamma ray from their nucleus; radioactivity distribution is estimated by detection of gamma rays. The most commonly used SPECT systems have one or more gamma camera “heads” (Devous et al., 1986; George et al., 1991; Holman and Devous, 1992; Masdeu et al., 1994; Devous, 1995). The gamma camera head has a large, relatively thin (e.g., 3/8 in by 12–20 in (0.96 cm by 30–50 cm) diameter) scintillation crystal of sodium iodide, which gives off a localized pulse of light when it absorbs a gamma ray. The front of the crystal is covered with a parallel-hole collimator, which is typically made up of lead perforated by an array of small hexagonal holes. The collimator limits the gamma rays that strike the crystal to those traveling along parallel lines perpendicular to the crystal face. An array of photomultiplier tubes and position logic circuits behind

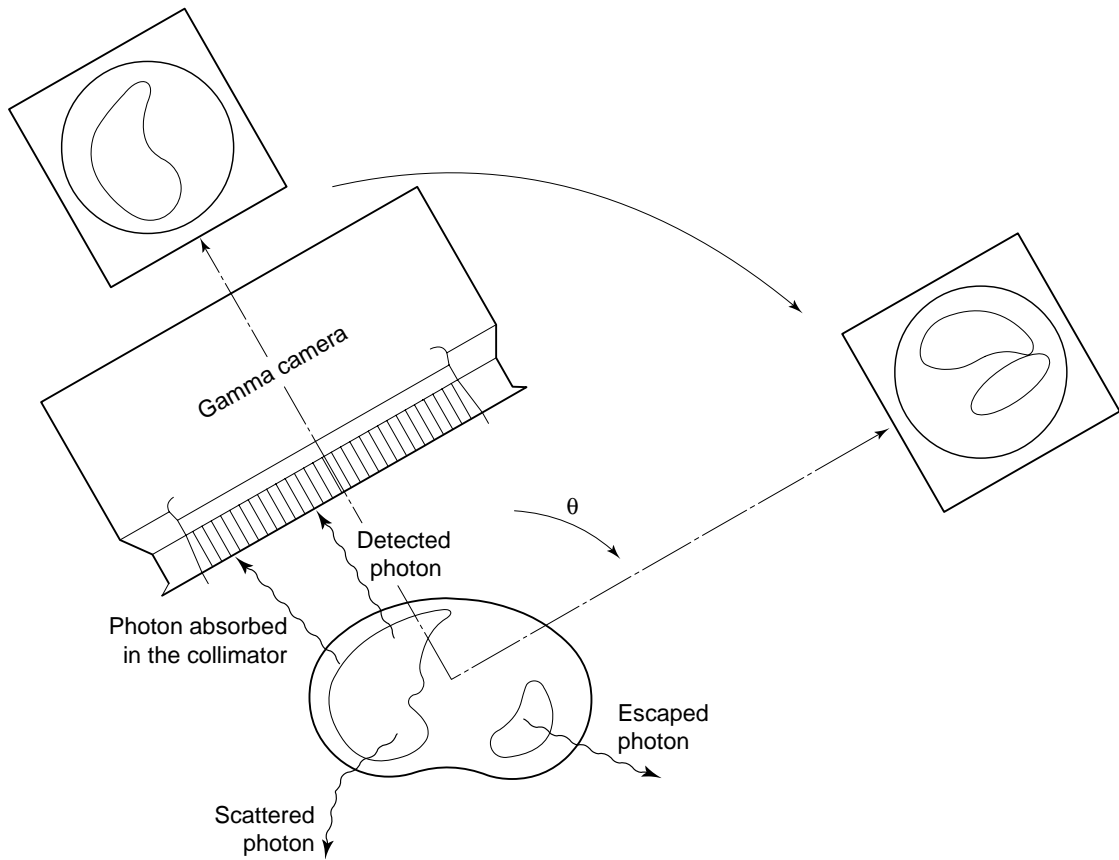


Fig. 1.5. SPECT data acquisition with a gamma camera. The collimator and the thin sodium iodide crystal detector behind the collimator are shown. Gamma rays or photons pass through the parallel holes in the collimator to the crystal and are registered by photomultipliers and electronic circuitry behind the crystal. Some photons strike the collimator septa at an angle and are absorbed, while others escape the body away from the view of the camera head and are not detected. As the head rotates around the patient, images are collected at each scanning angle. Scan profiles from these images are used as input for the SPECT reconstruction algorithm to obtain tomographic images of the distribution of radioactivity in the body. (From Sorenson and Phelps, 1987, with permission.)

the crystal sense the light pulses and determine the location of each pulse in the crystal. This information is used to generate a planar image of the distribution of radioactivity in the body. In order to obtain tomographic images, the camera head is rotated around the body to obtain multiple views (Fig. 1.5). These are combined to reconstruct tomographic images of the radioactivity distribution. To improve sensitivity, modern systems have two or three heads, mounted in a gantry, that surround the body and rotate together. Alternative SPECT designs, which are in limited use, employ either a circumferential array of small detectors or a single continuous cylindrical crystal that surrounds the patient (Holman et al., 1990).

SPECT devices have a spatial resolution of about 15 mm with single heads, and 6–9 mm with multiple heads and

different collimator designs. Sensitivity tends to be low, even with multiple head devices, because of the need for collimators; as a result, the imaging time is typically 20–30 min and radiotracers that provide a static unchanging distribution are typically used. Unlike PET, an accurate measured correction for attenuation is not convenient, and in some camera configurations is not possible at all. The methods currently used provide only an approximate attenuation correction (Bailey, 1998), and thus limit the absolute quantification of regional radioactivity. Typically, radioactivity is not quantified in absolute terms, but rather the tomographic images are used to obtain information about the relative concentration of radioactivity in different regions. A major advantage is that single-headed cameras with SPECT capability are ubiquitous in nuclear

medicine departments, and multi-headed systems have become more widespread. In addition, a cyclotron is not required to produce SPECT radiopharmaceuticals. The cost of SPECT instruments at the end of the 1990s ranges from \$250 000 to \$1 000 000, depending primarily upon the number of heads; in contrast PET scanners cost about \$2 500 000 (and, additionally, the cyclotron needed to produce PET radionuclides itself costs about \$1 500 000).

Radiotracer methods

Most SPECT brain studies are performed with radiopharmaceuticals that map CBF. Several radiopharmaceuticals are available for this purpose (George et al., 1991; Holman and Devous, 1992; van Heertum et al., 1993). The most commonly used radiotracer strategy is based on the microsphere method, a technique used to measure local flow in experimental animals (Warner et al., 1987). With that method, radioactive microspheres of a size appropriate to be trapped in capillaries are introduced into the left side of the animal's heart. They are distributed and trapped in tissue in proportion to flow and then local radioactivity is measured in samples of tissue. SPECT uses lipophilic radiotracers with microsphere-like behavior that are administered intravenously. Ideally they are freely diffusible across the blood-brain barrier and are completely extracted and retained by brain in a distribution that is proportional to local flow. The tracers have a stable distribution in the brain, facilitating imaging. Several SPECT perfusion agents are based on this principle, although their extraction or retention by brain is not complete (Gemmell et al., 1992).

The first widely used SPECT CBF tracer was [^{123}I]-iodoamphetamine ([^{123}I]-IMP). It must be pre-labeled by the commercial supplier, however, which is logistically difficult. Tracers using $^{99\text{m}}\text{Tc}$ are preferable because $^{99\text{m}}\text{Tc}$ is more convenient to use: it is obtained from generators that are delivered regularly to nuclear medicine departments; thus on-site labeling is possible. In addition, the physical characteristics of its radioactive decay are more favorable for SPECT imaging. A widely used $^{99\text{m}}\text{Tc}$ CBF agent is [$^{99\text{m}}\text{Tc}$]-labeled hexamethylpropylene amine oxime (also called [$^{99\text{m}}\text{Tc}$]-exametazime, [$^{99\text{m}}\text{Tc}$]-HMPAO). Another compound, [$^{99\text{m}}\text{Tc}$]-labeled ethyl cysteinate dimer [$^{99\text{m}}\text{Tc}$]-bicisate, [$^{99\text{m}}\text{Tc}$]-ECD, is replacing HMPAO. ECD provides higher brain-to-background radioactivity ratios because of more rapid blood clearance and is more convenient to employ because of greater in vitro stability. Although there are methods to calculate absolute rCBF with these tracers that use arterial blood sampling and a tracer kinetic model (Greenberg et al., 1990; Murase et al., 1992), they are rarely

used. As a result, SPECT studies typically provide information about relative rCBF, not absolute rCBF.

SPECT studies are relatively easy to perform since the scanners are widely available and they do not require an in-house cyclotron to produce the radiotracer. The distribution of radiotracer in brain reflects the blood flow during the first few minutes after injection of the tracer and remains relatively stable. Therefore, scanning can start up to 30 min after tracer injection and it is not necessary to inject the tracer while the subject is in the scanner. Repeat SPECT studies cannot be performed rapidly because the half-life of $^{99\text{m}}\text{Tc}$ is 6 h, unless methods are used to subtract residual radioactivity. SPECT perfusion studies have been performed in the pediatric age group, and even in newborn infants (Borch and Greisen, 1997). It is also possible to measure rCBV with SPECT using [$^{99\text{m}}\text{Tc}$]-labeled red cells (Kuhl et al., 1980); the approach is similar to that used for PET. However, there are no SPECT radiotracers to study cerebral metabolism.

Recently, there has been considerable progress in the development of receptor-binding ligands for SPECT, especially for dopamine and benzodiazepine receptors (Holman and Devous, 1992) and for dopamine reuptake transporters (Seibyl et al., 1996) (Table 1.2). Iodine-123 is typically used to label these ligands. The techniques of tracer kinetic modeling described above are applied to analyze image and blood radioactivity data (Laruelle et al., 1994a,b).

Data analysis

After a PET study has been completed, the relevant tracer model is applied to calculate the physiologic variable of interest. For the methods to measure cerebral hemodynamics and metabolism described above, the model is applied on a point-by-point basis and the intensity of the resultant image depends upon the local value of the physiologic measurement (see Fig. 1.4). Although visual inspection of PET images may reveal abnormalities, quantitative analysis and appropriate statistical techniques are required for clinical research. Data reduction, analysis, and interpretation are very demanding. Newer scanners acquire up to 63 slices simultaneously, each containing data from many brain structures. Several scans of the same or different types may be obtained in one session, for example multiple rCBF scans, or rCBF and rCMRglu scans, and subjects may have repeat studies on different days. The analysis of PET data is greatly facilitated by interactive computer programs. These programs permit regions of interest (ROIs) of arbitrary size and shape to be placed over

Table 1.2. Representative SPECT radiotracers

Physiologic process or system	Radiotracer
<i>Cerebral blood flow</i>	[¹²³ I]-Iodoamphetamine ([¹²³ I]-IMP) [^{99m} Tc]-labeled exametazime ([^{99m} Tc]-HMPAO) [^{99m} Tc]-labeled ethyl cysteinate dimer ([^{99m} Tc]-ECD)
<i>Cerebral plasma and red cell volume</i>	[^{99m} Tc]-labeled human serum albumin [^{99m} Tc]-labeled red blood cells
<i>Neuroreceptor systems</i>	
Dopaminergic	
Dopamine D ₂ receptors	[¹²³ I]-Iodobenzamide ([¹²³ I]-IBZM); [¹²³ I]-epidepride
Dopamine D ₁ receptors	[¹²³ I]-SCH23982
Dopamine reuptake sites	[¹²³ I]-N-(3-Fluoropropyl)-2β-carbomethoxy-3β-(4-iodophenyl)nortropine ([¹²³ I]-β-CIT)
Benzodiazepine	[¹²³ I]-Iomazenil
Cholinergic muscarinic	[¹²³ I]-Labeled quinuclidinylbenzilate [¹²³ I]-QNB; [¹²³ I]-iododexetimide
Serotonergic 5-HT _{2A} receptors	[¹²³ I]-R93274
<i>Amino acid transport</i>	[¹²³ I]-Iodo-α-methyltyrosine

different structures for which the physiologic variable is then computed. Also, whole-brain measurements can be obtained by averaging over several PET slices, or by using a template of ROIs to sample multiple brain regions.

PET measurements must be related to the underlying anatomy. Early approaches to data analysis used PET images obtained in standard planes, for example parallel to the canthomeatal line. The images were visually compared to corresponding anatomic sections in a brain atlas and the ROIs manually drawn. This method, however, is subjective and liable to observer bias. A refinement uses a template of standard regions to sample brain structures of interest, with visual adjustment to fit the template to the images. Alternative approaches have been developed that relate PET images to anatomy more accurately and objectively. A widely used approach uses the principles of stereotactic localization to establish a correspondence between brain areas or volumes in a stereotactic brain atlas and specific regions or pixels in the PET image (Fox et al., 1985; Friston et al., 1989). Other methods are required if there are structural abnormalities. An approach widely used for both normal and abnormal brain is to obtain anatomic images with CT or MRI in the same planes as the PET slices. Methods to achieve this include head holders transferable between imaging modalities, fiducial markers affixed to the head, and, most conveniently, automated computer techniques to register and reslice PET and MR or CT images (Pelizzari et al., 1989; Wilson and Mountz, 1989; Evans et al., 1991; Woods et al., 1993; Ge et al., 1994). After coplanar anatomic and PET images have been obtained,

ROIs can be transferred between them. These automated techniques have also been used to register brain SPECT images with CT or MR images (Holman et al., 1991).

A variety of sophisticated methods have been developed to extract information from functional brain images. One approach consists of calculating the relationship between CBF or metabolism in multiple pairs of brain regions (Horwitz et al., 1992). A high degree of correlation or covariance between the activity in two brain regions is attributed to a high level of functional connectivity or coupling between them during a particular condition (Friston, 1994). This implies that the regions work together, influence each other, or are affected in a similar fashion by a third region. In a refinement of this approach called path analysis, knowledge of the neuroanatomic connections between brain areas is included in the computation of interregional correlations, and functional networks consisting of several brain regions can be identified (McIntosh et al., 1994). An alternative group of approaches, including principle components analysis and scaled subprofile modeling, attempts to identify groups of regions that account for the variability in a dataset and which may be functionally related (Strother et al., 1995).

The technique of statistical parametric mapping (SPM) has become a widely applied method. It is typically used to determine the difference, on a pixel-by-pixel basis, between sets of rCBF images obtained in different study conditions (Friston et al., 1991; Frackowiak and Friston, 1994; Acton and Friston, 1998). This method basically consists of three steps. The first is image normalization in

which each pixel is mapped into the same stereotactic space; thus all pixels in the image set are transformed into a common reference brain in a 3D coordinate system. This permits the second step, that is averaging images obtained from different subjects studied during the same condition. This reduces image noise and facilitates the detection of significant differences between conditions. Because image noise in PET images is random, it decreases when images are averaged, while the rCBF pattern, which is consistent across subjects, remains. The final step is to perform statistical tests on a pixel-by-pixel basis between datasets to identify regions of significant rCBF change. The results are displayed as 3D maps or views of the reference brain in which pixels with a significant change in rCBF are highlighted.

SPM was originally designed to determine the changes in local CBF measured with $H_2^{15}O$ in subjects studied during two or more different neurobehavioral tasks in functional brain mapping experiments. It can also be applied in a parametric analysis to see which brain regions covary in a systematic fashion with some parameter related to the performance of a cognitive, sensory, or motor task (e.g., the rate of hand movement). SPM has subsequently been applied to both $H_2^{15}O$ and FDG images in other types of study, for example before and after administration of a drug or to compare a group of patients with a control group. It has also been used to analyze perfusion images obtained with SPECT (Acton and Friston, 1998).

There is variability in both regional and global PET measurements. The coefficient of variation (i.e., the ratio of the standard deviation to the mean value) for measurements of rCBF, rCMRGlucose, and rCMRO₂ is 15–25% in groups of normal subjects (Perlmutter et al., 1987; Tyler et al., 1988; Camargo et al., 1992; Wang et al., 1994), although the variability in repeat measurements in the same subject is less (Matthew et al., 1993). This may reflect normal physiologic variation or methodologic inaccuracies. Approaches have been developed to facilitate detecting regional changes in spite of this variability. These adjust for the effect of global variations by “normalizing” regional data, thereby decreasing their variance. This can be done by dividing regional values by the global average value or by the value in a structure presumed to be minimally involved in the disease being studied. Such techniques, however, can result in a loss of the information contained in the absolute values, especially if widespread changes occur. If the denominator as well as the numerator differs between groups, erroneous conclusions may be drawn. For example, in a study of Alzheimer’s disease (Cutler et al., 1985), normalized rCMRGlucose in thalamus was significantly *increased* because of a *decrease* in global metabolism. In other words, the

metabolism in the thalamus may be relatively spared. Therefore, normalized PET data must be carefully interpreted. In spite of the variability of PET measurements, it is possible to demonstrate meaningful physiologic abnormalities with absolute data, for example in cerebrovascular disease (Powers, 1998).

SPECT perfusion studies typically do not involve quantitation of absolute rCBF. Although the image intensity is proportional to flow, it also depends on the amount of tracer reaching the brain, which can vary between patients and even in the same patient because of variations in the peripheral circulation as well as body size. A normalization procedure is performed if regional tissue count data are to be averaged in a patient group or compared with data from normal subjects. This is accomplished by dividing the count data in individual ROIs by the average count value (Goldenberg et al., 1992) or by the value in the cerebellum, assuming that it is not involved in the disease process. There are potential ambiguities with this approach. For example, a region with the appearance of increased perfusion may actually have an elevated flow, but the finding may also reflect reduced flow in other brain regions (Wilson and Wyper, 1992).

Data from control subjects are required to interpret PET or SPECT measurements obtained in patients. Quantitative data obtained in appropriately selected normal subjects are used. Depending on the nature of the study, selection criteria must control for variables such as age, gender, handedness, and condition of general health; in children, sexual and cognitive maturation must also be included. Average data from patients are statistically compared with the same regional measurements made in a group of normal control subjects. It is also possible to analyze regional data obtained in an individual patient, for example by determining whether they are outside the range of normal. In comparing measurements obtained from many brain regions, it is possible that some regions will be found to be significantly different by chance because of the large number of multiple comparisons being made. One approach to avoid this error, which is rather conservative, is to adjust the study *p* value (typically 0.05) by dividing it by the number of measurements being made (the Bonferroni correction).

One must also consider the possibility of a drift in measurements over years in the case of longitudinal studies, which have a special place in pediatric research. Usually, these changes over time caused by subtle changes in scanner performance can be corrected by covariance analysis. This stresses the importance of systematic and rigorous quality control of scanners and the interleaving of patients and controls over the duration of a study.

If visual analysis of SPECT and PET images is used, it requires a rigorous approach. SPECT images are frequently interpreted visually for abnormalities. The criteria for defining an abnormality are usually subjective, however, and further work must be done to define the sensitivity and specificity for detecting abnormalities (Juni, 1994; Stapleton et al., 1994). In some SPECT studies, there is a clear definition of regional abnormality and scans are graded by agreement among two or more observers (Jacobs et al., 1994), whereas other studies have used less careful methodology. This makes it difficult to compare different studies.

Interpretation of changes in cerebral blood flow and metabolism

Physiologic considerations

To interpret changes in PET and SPECT studies, it is necessary to understand the relationships among CBF, metabolism, and local neuronal activity, and the mechanisms by which CBF and metabolism can become abnormal.

Normally, about 30% of the brain's energy metabolism supports synaptic transmission, 30% residual ion fluxes and transport, and 40% other processes such as axoplasmic transport and macromolecular synthesis (Astrup et al., 1981). In the resting state, the energy needs of the brain are met by the oxidative metabolism of glucose, and there is a proportional relationship, termed coupling, between rCBF and both rCMRO₂ and rCMRGlucose (Sokoloff, 1981; Baron et al., 1984; Fox and Raichle, 1986; Fox et al., 1988). During increased local neuronal activity, for example with somatosensory or visual stimulation, there are coupled or parallel increases in rCBF and rCMRGlucose in the brain regions involved (Sokoloff, 1961; Leniger-Follert and Hossman, 1979; Toga and Collins, 1981; Yarowsky et al., 1983; Fox and Raichle, 1984; Ginsberg et al., 1987; Fox et al., 1988). Within physiologic limits, these increases parallel the stimulus rate and the rate of neuronal firing. Most of the brain's additional glucose consumption during increased neuronal activity is used to maintain ionic gradients across cell membranes, which must be restored after depolarization (Yarowsky and Ingvar, 1981). These observations form the basis for using measurements of rCBF and rCMRGlucose as markers of local neuronal function (Raichle, 1987). PET studies in humans have shown, however, that there is only a slight increase in rCMRO₂ during functional activation (Fox and Raichle, 1986; Fox et al., 1988). This observation challenged the hypothesis that oxidative glucose metabolism or its products regulate the rCBF changes during neuronal activation. In fact, the processes responsible for

coupling rCBF to rCMRGlucose at rest and during activation remain to be elucidated (Lou et al., 1987; Raichle, 1991; Edvinsson et al., 1993b; Jueptner and Weiller, 1995).

Various mechanism can lead to abnormalities of CBF and metabolism. Changes in neuronal activity can result in increases or decreases in local CBF and metabolism. Decreased neuronal activity in coma decreases CBF and metabolism (Obrist et al., 1984), as can drugs and anesthetics that act on synapses or membranes to depress neuronal activity. Abnormalities in blood flow and metabolism in specific brain regions have been found in many neurologic and psychiatric diseases. These may reflect altered neuronal activity either in the area(s) of abnormality or in distant brain regions that project to the area(s). In many diseases, several brain areas are affected, implying an abnormality in underlying brain networks. Both acute and chronic administration of drugs have been shown to change rCBF and metabolism. These changes have been related to the action of the drug on a specific receptor system with a resulting change in activity.

Tissue damage or loss, either gross or through loss of neurons, can decrease flow and metabolism. In addition, coupled decreases in flow and metabolism can be seen in structures *distant* to a lesion. This phenomenon, called diaschisis, is attributed to a decrease in neuronal activity in a brain structure through loss of afferent projections from the damaged region (Feeney and Baron, 1986). For example, decreased flow and metabolism can be seen in the cerebellum contralateral to a cerebral infarct. There are situations when flow and metabolism are not coupled, for example with changes in arterial blood gases (Edvinsson et al., 1993a) and in pathologic conditions such as cerebrovascular disease (Powers, 1988, 1991; Heiss and Podreka, 1993) or elevated intracranial pressure (Grubb et al., 1975).

Effect of limited spatial resolution

Artificial abnormalities of CBF and metabolism can be observed with PET or SPECT because of the limited spatial resolution of the imaging devices. Limited resolution results in blurring of PET and SPECT images (Fig. 1.6). More important is its effect on the accuracy of radioactivity measurement (Hoffman et al., 1979; Mazziotta et al., 1981). Because the radioactivity appears spread out over a larger area, a brain region in the image contains only a portion of the radioactivity that was in the corresponding brain structure. In addition, some of the radioactivity in surrounding structures appears to be spread into the region. Because of this effect, called partial volume averaging, a regional measurement contains a contribution from both the structure of interest and surrounding struc-

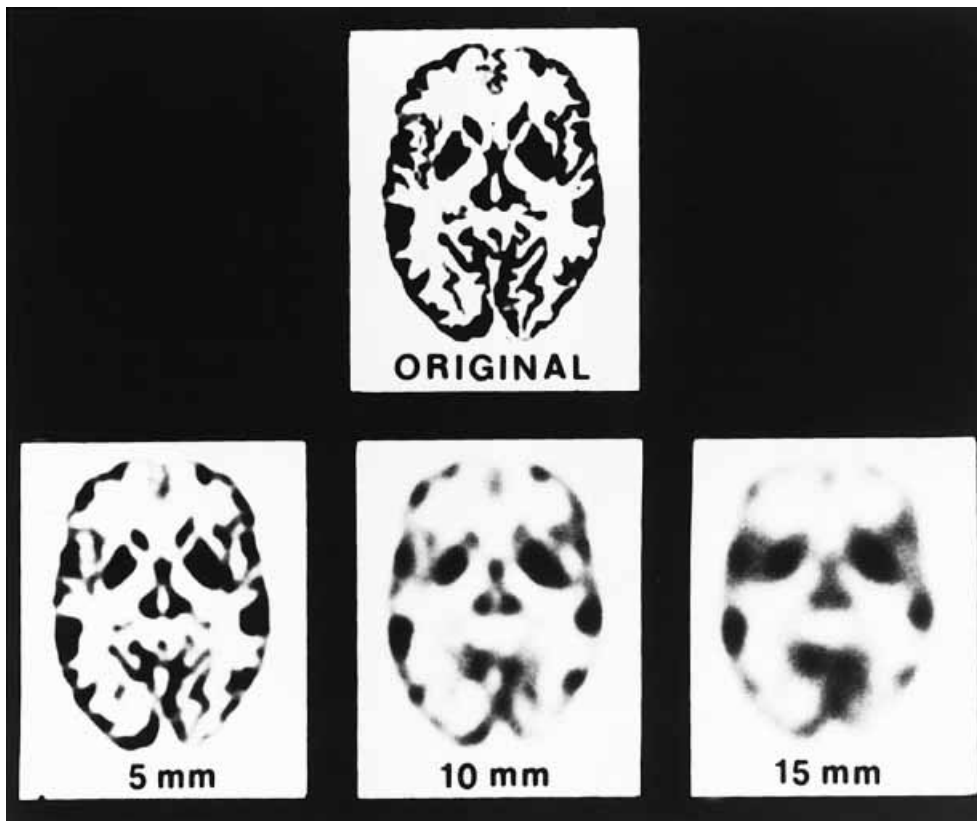


Fig. 1.6. The effect of scanner resolution on the accuracy of images obtained. At the upper center is a simulated “ideal” PET image of regional radioactivity, reflecting the higher metabolic activity in gray matter. Subsequent images simulate the effect of obtaining this image with tomographs of varying spatial resolution, from 5 to 15 mm FWHM (full width at half maximum). Note the blurring or spreading out of radioactivity, with gray matter structures appearing paler. As a result, radioactivity in cortical and subcortical gray matter regions is underestimated. Similar considerations hold for SPECT images. (From Mazziotta et al., 1981, with permission.)

tures. High radioactivity levels surrounded by lower values will be underestimated, while low radioactivity surrounded by high activity will be overestimated. These errors are less when the size of the structure of interest is large with respect to scanner resolution. In a circular, uniform structure with a diameter twice the resolution, the radioactivity concentration will be accurately represented in the center. However, statistical considerations limit obtaining a measurement with a very small ROI. In general, it is not possible to measure pure gray matter radioactivity, especially in thin cortical regions.

Partial volume averaging with cerebrospinal fluid in sulci or ventricles can lead to an underestimation of tissue blood flow and metabolism. If there is cerebral atrophy, PET and SPECT measurements will be further reduced because of partial volume averaging with enlarged, metabolically inactive, cerebrospinal fluid spaces (Herscovitch et al., 1986; Videen et al., 1988). Beyond the border of a circumscribed

region of decreased flow or metabolism, one would observe a gradual transition of the physiologic measurement to the value in surrounding normal tissue, also caused by partial volume averaging (Powers, 1988). This gives rise to the false perception that the PET or SPECT “lesion” is larger than the actual abnormality. Recently, decreased CBF and metabolism in the subgenual prefrontal cortex in patients with familial depression was found to be associated with a focal reduction in gray matter volume of the affected cortical structure. This intriguing observation indicates that altered PET measurements can be found through partial volume averaging in conditions with an unsuspected anatomic abnormality (Drevets et al., 1997).

Methods have been developed to correct for partial volume averaging and recover a more accurate radioactivity measurement from small brain structures (Meltzer et al., 1996), and these should find increasing application. The contribution of partial volume effect is particularly

important in the developing brain where size, shape, and homogeneity of structures vary with neural maturation (Giedd et al., 1996a, b; Rajapakse et al., 1996).

Effect of patient motion

Head movement is particularly important when subjects are children who have trouble remaining immobile. Motion between the transmission and emission scans can lead to a mismatch in the attenuation correction factors. Motion during an emission can blur the image in a nonuniform manner and increase partial volume errors. Motion between scans obtained at rest and during performance of a task in a given subject can lead to artefactual differences between the scans being interpreted as activation. The relative impact of this blurring becomes greater as the resolution of the scanner improves.

Head motion during brain scans can be reduced with a variety of head support or stabilization devices, but it cannot be entirely eliminated. Several methods of detecting and correcting for motion have been developed. One technique is based on radioactive fiducial markers that are used to align scans of short duration, which are then summed (Koeppel et al., 1991). Another method employs the images of the brain themselves to estimate the corrections necessary to obtain maximum alignment of the serial images (Minoshima et al., 1992).

Radiation exposure and technical issues in pediatric imaging

Radiation exposure

Although the short half-lives of PET radionuclides favourably affects the radiation exposure to subjects, this exposure is not negligible. Radiation exposure in the context of PET and SPECT is an important consideration when they are used for research rather than diagnostic purposes (Veatch, 1982; Huda and Scrimger, 1989). Limits on radiation exposure to research subjects are set by regulatory bodies such as the US Food and Drug Administration and institutional radiation safety committees. The potential risks associated with low levels of radiation such as those received from PET are carcinogenesis and genetic effects in future generations (Brill, 1987). Although the risk is very low (for review, see Ernst et al., 1998), it is agreed that the least amount of radiotracer necessary to perform an adequate PET study should be administered.

Methods have been developed to determine radiation exposure from internally administered radiopharma-

ceuticals (Cloutier and Watson, 1987; Loevinger et al., 1988; Kassis, 1992). The distribution of the radiotracer in the body is first determined as a function of time following its administration. This information can be calculated using physiologic models of in vivo tracer behavior, extrapolated from measurements in animals, or measured in a small group of human subjects. Then the radiation exposure to each organ is calculated using a model of the body that simulates the size, shape, and properties of body organs. Appropriate models have been designed for the pediatric age group, including the neonate.

Regulations in the USA typically restrict radiation exposure in minors participating in research studies to one-tenth that allowed in adults. The use of newer, 3D PET scanners has improved the situation with regard to radiation exposure in pediatric PET studies. Because of the greater sensitivity of these scanners, it is possible to administer smaller doses of radiotracer and maintain image quality. In addition, in some cases specific strategies can be employed to reduce radiation exposure. For example, in FDG studies one can have the subject void after the 30–45 min uptake period rather than after the completion of emission scanning, to reduce radiation exposure to the urinary bladder, the organ that receives the greatest radiation exposure (Zametkin et al., 1993) (see Chapter 6).

Technical issues

Clinical research with PET is more complex in the pediatric age group than in adults for several reasons.

Measurement of radioactivity in arterial blood is typically required to perform truly quantitative studies. In the adult, arterial catheters can routinely be inserted purely for research purposes (Lockwood, 1985), but this is a major obstacle in minors. In sick infants, arterial samples have been obtained from catheters previously placed for intensive care purposes (Volpe et al., 1983). There are alternatives, however. For FDG studies, venous sampling can be performed from a hand heated to 44°C to “arterialize” venous blood (Phelps et al., 1979); this does require cooperation from the subject. With certain PET tracer techniques, the image of local radioactivity is approximately proportional to the underlying physiologic variable, for example rCBF with a bolus intravenous injection of $H_2^{15}O$, or rCMRGlucose with FDG. With appropriate data analysis strategies, information about regional abnormalities can be obtained without blood sampling.

A novel approach to obtaining the arterial time–radioactivity curve involves imaging the heart after injection of tracer. Multiple brief scans are obtained, and the blood curve is measured using an ROI placed over the left

ventricle. This approach was originally applied to PET studies of the heart, where both the heart chamber and the tissue of interest (the myocardium) are simultaneously in the field of view of the scanner (Weinberg et al., 1988; Bergmann et al., 1989; Iida et al., 1992). It can also be used with certain radiotracer techniques that are used to study the brain, for example with FDG or [^{11}C]- α -methyltryptophan (Muzik et al., 1998), for which there is a prolonged tracer uptake period that is followed by emission imaging of the brain.

During a PET scan, it is necessary to prevent head movement. In cooperative adults, this is accomplished by means of a specially designed headholder affixed to the scanner couch. Children may find this difficult to tolerate. For the FDG method, it is possible to sedate the subject for the emission image after the 30–45 min tracer uptake period, because the tracer distribution in brain has already been established. Also, for scans that require prolonged imaging, it is possible to collect the data in multiple brief scans that can be spatially registered to each other to correct for head movement.

Although normal adults are frequently scanned to obtain control data for comparison with patient data, it is usually difficult to scan normal children in PET or SPECT studies because of ethical considerations (Chapter 6). Depending upon the research question, some studies do not require control data (e.g., Altman et al., 1989; Perlman and Altman, 1992). For studies that require normal control data, a suboptimal approach can be used: the control group can include retrospectively selected children who had been scanned for appropriate clinical research indications, such as a neurologic event thought not to affect brain development or diagnostic evaluation for a neurologic disease that is ultimately excluded (Chugani and Phelps, 1991; Bentourkia et al., 1998; van Bogaert et al., 1998). Another strategy is to enroll healthy siblings of children affected by the condition being studied because the siblings have the possibility of indirect benefit from increased knowledge of the condition. The issue of studying normal children is discussed further in Chapter 6.

References

- Acton, P. D. and Friston, K. J. (1998). Statistical parametric mapping in functional neuroimaging: beyond PET and fMRI activation studies. *Eur. J. Nucl. Med.*, **25**, 663–7.
- Altman, D. I., Perlman, J. M., Volpe, J. J. and Powers, W. J. (1989). Cerebral oxygen metabolism in newborn infants measured with positron emission tomography. *J. Cereb. Blood Flow Metab.*, **9**(Suppl. 1), S25.
- Altman, D. I., Lich, L. L. and Powers, W. J. (1991). Brief inhalation method to measure cerebral oxygen extraction with PET: accuracy determination under pathologic conditions. *J. Nucl. Med.*, **32**, 1738–41.
- Astrup, J., Sorensen, P. M. and Sorensen, H. R. (1981). Oxygen and glucose consumption related to Na^+ - K^+ transport in canine brain. *Stroke*, **12**, 726–30.
- Bailey, D. L. (1998). Transmission scanning in emission tomography. *Eur. J. Nucl. Med.*, **25**, 774–87.
- Bailey, D. L., Miller, M. P., Spinks, T. J. et al. (1998). Experience with fully 3D PET and implications for future high-resolution 3D tomographs. *Phys. Med. Biol.*, **43**, 777–86.
- Baron, J. C., Rougemont, D., Soussaline, F. et al. (1984). Local interrelationships of oxygen consumption and glucose utilization in normal subjects and in ischemic stroke patients: a positron emission tomographic study. *J. Cereb. Blood Flow Metab.*, **4**, 140–9.
- Baron, J. C., Frackowiak, R. S. J., Herholz, K. et al. (1989). Use of PET methods for measurement of cerebral energy metabolism and hemodynamics in cerebrovascular disease. *J. Cereb. Blood Flow Metab.*, **9**, 723–42.
- Bentourkia, M., Michel, C., Ferriere, G. et al. (1998). Evolution of brain glucose metabolism with age in epileptic infants, children and adolescents. *Brain Dev.*, **20**, 524–9.
- Bergmann, S. R., Herrero, P., Markham, J., Weinheimer, C. J. and Walsh, M. N. (1989). Noninvasive quantitation of myocardial blood flow in human subjects with oxygen-15-labeled water and positron emission tomography. *J. Am. Coll. Cardiol.*, **14**, 639–52.
- Bergstrom, M., Eriksson, L., Bohm, C., Blomqvist, G. and Litton, J. (1983). Correction for scattered radiation in a ring detector positron camera by integral transformation of the projections. *J. Comput. Assist. Tomogr.*, **7**, 42–50.
- Berridge, M. S., Adler, L. P., Nelson, A. D. et al. (1991). Measurement of human cerebral blood flow with [^{15}O]butanol and positron emission tomography. *J. Cereb. Blood Flow Metab.*, **11**, 707–15.
- Blomqvist, G., Stone-Elander, S., Halldin, C. et al. (1990). Positron emission tomographic measurements of cerebral glucose utilization using [^{11}C]D-glucose. *J. Cereb. Blood Flow Metab.*, **11**, 467–83.
- Borch, K. and Greisen, G. (1997). $^{99\text{m}}\text{Tc}$ -HMPAO as a tracer of cerebral blood flow in newborn infants. *J. Cereb. Blood Flow Metab.*, **17**, 448–54.
- Brill, A. B. (1987). Biological effects of ionizing radiation. In *Nuclear Medical Physics*, ed. L. E. Williams, pp. 163–83. Boca Raton, FL, CRC Press.
- Brooks, R. A. (1982). Alternative formula for glucose utilization using labeled deoxyglucose. *J. Nucl. Med.*, **23**, 583–9.
- Budinger, T. F., Derenzo, S. E., Greenberg, W. L., Gullberg, G. T. and Huesman, R. H. (1978). Quantitative potentials of dynamic emission computed tomography. *J. Nucl. Med.*, **19**, 309–15.
- Camargo, E. E., Szabo, Z., Links, J. M. et al. (1992). The influence of biological and technical factors on the variability of global and regional brain metabolism of 2- ^{18}F fluoro-2-deoxy-D-glucose. *J. Cereb. Blood Flow Metab.*, **12**, 281–90.
- Carson, R. E. (1991). Precision and accuracy considerations of physiological quantitation in PET. *J. Cereb. Blood Flow Metab.*, **11**, A45–50.

- Carson, R. E. (1996). Mathematical modeling and compartmental analysis. In *Nuclear Medicine*, ed. J. C. Harbert, W. E. Eckelman and R. D. Neumann, pp. 167–93. New York: Thieme.
- Carson, R. E., Daube-Witherspoon, M. E. and Green, M. V. (1988). A method for postinjection PET transmission measurements with a rotating source. *J. Nucl. Med.*, **29**, 1558–67.
- Cherry, S. R., Chatziioannou, A., Shao, Y., Silverman, R. W., Meadors, K. and Phelps, M. E. (1998). Brain imaging in small animals using MicroPET, In *Quantitative Functional Brain imaging with Positron Emission Tomography*, ed. R. E. Carson, M. E. Daube-Witherspoon and P. Herscovitch, pp. 201–6. San Diego, CA: Academic Press.
- Chugani, H. T. and Phelps, M. E. (1991). Imaging human brain development with positron emission tomography [editorial comment]. *J. Nucl. Med.*, **32**, 23–6.
- Cloutier, R. J. and Watson, E. E. (1987). Internal dosimetry – an introduction to the ICRP technique. In *Nuclear Medical Physics*, ed. L. E. Williams, p. 143. Boca Raton, FL: CRC Press.
- Council on Scientific Affairs (1988). Instrumentation in positron emission tomography. *J. Am. Med. Assoc.*, **259**, 1351–6.
- Cunningham, V. and Cremer, J. E. (1985). Current assumptions behind the use of PET scanning for measuring glucose utilization in brain. *Trends Neurosci.*, **8**, 96–9.
- Cutler, N. R., Haxby, J. V., Duara, R. et al. (1985). Clinical history, brain metabolism, and neuropsychological function in Alzheimer's disease. *Ann. Neurol.*, **18**, 298–309.
- Dannals, R. F., Ravert, H. T. and Wilson, A. A. (1993). Chemistry of tracers for positron emission tomography. In *Nuclear Imaging in Drug Discovery, Development, and Approval*, ed. D. H. Burns, R. E. Gibson, R. F. Dannals and P. K. S. Siegl, pp. 55–74. Boston: Birkhäuser.
- Daube-Witherspoon, M. E. and Herscovitch, P. (1996). Positron emission tomography. In *Nuclear Medicine*, ed. J. C. Harbert, W. E. Eckelman and R. D. Neumann, pp. 121–43. New York: Thieme.
- de Grado, T. R., Turkington, T., Williams, J. J., Stearns, C. W., Hoffman, J. M. and Coleman, R. E. (1994). Performance characteristics of a whole-body PET scanner. *J. Nucl. Med.*, **35**, 1398–1406.
- Devous, M. D., Stokely, E. M., Chehabi, H. H. and Bonte, F. J. (1986). Normal distribution of regional cerebral blood flow measured by dynamic single-photon emission tomography. *J. Cereb. Blood Flow Metab.*, **6**, 95–104.
- Devous, M. D. (1995). SPECT functional brain imaging: technical considerations. *J. Neuroimaging*, **5**(Suppl. 1), S2–13.
- Drevets, W. C., Price, J. L., Simpson, J. R. et al. (1997). Subgenual prefrontal cortex abnormalities in mood disorders. *Nature*, **386**, 824–7.
- Edvinsson, L., MacKenzie, E. T. and McCulloch, J. (1993a). Changes in arterial gas tensions. In *Cerebral Blood Flow and Metabolism*, pp. 524–52. New York: Raven Press.
- Edvinsson, L., MacKenzie, E. T. and McCulloch, J. (1993b). Neurotransmitters: metabolic and vascular effects in vivo. In *Cerebral Blood Flow and Metabolism*, pp. 159–80. New York: Raven Press.
- Eriksson, L., Holte, S., Bohm, C., Kesselberg, M. and Hovander, B. (1988). Automated blood sampling systems for positron emission tomography. *IEEE Trans. Nucl. Sci.*, **35**, 703–7.
- Ernst M., Freed M. E. and Zametkin, A. J. (1998). Health hazards of radiation exposure in the context of brain imaging research: special consideration for children. *J. Nucl. Med.*, **39**, 689–98.
- Evans, A. C., Marrett, S., Torrescorzo, J., Ku, S. and Collins, L. (1991). MRI-PET correlation in three dimensions using a volume-of-interest (VOI) atlas. *J. Cereb. Blood Flow Metab.*, **11**, A69–78.
- Feeney, D. M. and Baron, J. C. (1986). Diaschisis. *Stroke*, **17**, 817–30.
- Fowler, J. S. and Wolf, A. P. (1991). Recent advances in radiotracers for PET studies of the brain. In *Radiopharmaceuticals and Brain Pathology Studied with PET and SPECT*, ed. M. Diksic and R. C. Reba, pp. 11–34. Boca Raton, FL: CRC Press.
- Fox, P. T. and Raichle, M. E. (1984). Stimulus rate dependence of regional cerebral blood flow in human striate cortex, demonstrated by positron emission tomography. *J. Neurophysiol.*, **51**, 1109–20.
- Fox, P. T. and Raichle, M. E. (1986). Focal physiological uncoupling of cerebral blood flow and oxidative metabolism during somatosensory stimulation in human subjects. *Proc. Natl. Acad. Sci. USA*, **83**, 1140–4.
- Fox, P. T., Perlmutter, J. S. and Raichle, M. E. (1985). A stereotactic method of anatomical localization for positron emission tomography. *J. Comput. Assist. Tomogr.*, **9**, 141–53.
- Fox, P. T., Raichle, M. E., Mintun, M. A. and Dence, C. (1988). Nonoxidative glucose consumption during focal physiologic neural activity. *Science*, **241**, 462–4.
- Frackowiak, R. S. and Friston, K. J. (1994). Functional neuroanatomy of the human brain: positron emission tomography – a new neuroanatomical technique. *J. Anat.*, **184**, 211–25.
- Frackowiak, R. S. J., Lenzi, G.-L., Jones, T. and Heather, J. D. (1980). Quantitative measurement of regional cerebral blood flow and oxygen metabolism in man using ¹⁵O and positron emission tomography: theory, procedure and normal values. *J. Comput. Assist. Tomogr.*, **4**, 727–36.
- Friston, K. J. (1994). Functional and effective connectivity in neuroimaging: a synthesis. *Hum. Brain Map.*, **2**, 56–78.
- Friston, K. J., Passingham, R. E., Nutt, J. G., Heather, J. D., Sawle, G. V. and Frackowiak, R. S. J. (1989). Localisation in PET images: direct fitting of the intercommissural (AC-PC) line. *J. Cereb. Blood Flow Metab.*, **9**, 690–5.
- Friston, K. J., Frith, C. D., Liddle, P. F. and Frackowiak, R. S. J. (1991). Comparing functional (PET) images: the assessment of significant change. *J. Cereb. Blood Flow Metab.*, **11**, 690–9.
- Ge, Y. R., Fitzpatrick, J. M., Votaw, J. W. et al. (1994). Retrospective registration of PET and MR brain images – an algorithm and its stereotaxic validation. *J. Comput. Assist. Tomogr.*, **18**, 800–10.
- Gemmill, H. G., Evans, N. T. S., Besson, J. A. O. et al. (1992). Regional cerebral blood flow imaging: a quantitative comparison of technetium-99m-SPECT with C¹⁵O₂ PET. *J. Nucl. Med.*, **31**, 1595–1600.
- George, M. S., Ring, H. A., Costa, D. C., Ell, P. J., Kouris, K. and Jarritt, P. H. (1991). *Neuroactivation and Neuroimaging with SPECT*. London: Springer-Verlag.

- Giedd, J. N., Snell, J. W., Lange, N. et al. (1996a). Quantitative magnetic resonance imaging of human brain development: ages 4–18. *Cereb. Cortex*, **6**, 551–60.
- Giedd, J. N., Vaituzis, A., Hamburger, S. D. et al. (1996b). Quantitative MRI of the temporal lobe, amygdala, and hippocampus in normal development: ages 4–18 years. *J. Comp. Neurol.*, **366**, 223–30.
- Ginsberg, M. D., Dietrich, W. D. and Busto, R. (1987). Coupled fore-brain increases of local cerebral glucose utilization and blood flow during physiologic stimulation of a somatosensory pathway in the rat: demonstration by double-label autoradiography. *Neurology*, **37**, 11–19.
- Gjedde, A., Weinhard, K., Heiss, W.-D. et al. (1985). Comparative regional analysis of 2-fluorodeoxyglucose and methylglucose uptake in brain of four stroke patients. With special reference to the regional estimation of the lumped constant. *J. Cereb. Blood Flow Metab.*, **5**, 163–78.
- Goldenberg, G., Oder, W., Spatt, J. and Podreka, I. (1992). Cerebral correlates of disturbed executive function and memory in survivors of severe closed head injury: a SPECT study. *J. Neurol. Neurosurg. Psychiatry*, **55**, 362–8.
- Grafton, S. T. and Mazziotta, J. C. (1992). Cerebral pathophysiology evaluated with positron emission tomography. In *Diseases of the Nervous System: Clinical Neurobiology*, 2nd edn, ed. A. K. Asbury, G. M. McKhann and W. I. McDonald, pp. 1573–88. Philadelphia, PA: Saunders.
- Graham, M. M., Spence, A. M., Muzi, M. and Abbott, G. L. (1989). Deoxyglucose kinetics in a rat brain tumor. *J. Cereb. Blood Flow Metab.*, **9**, 315–22.
- Green, M. V. (1996). Single photon imaging. In *Nuclear Medicine*, ed. J. C. Harbert, W. E., Eckelman and R. D. Neumann, pp. 87–120. New York: Thieme.
- Greenberg, J. H., Kushner, M., Rangno, M., Alavi, A. and Reivich, M. (1990). Validation studies of iodine-123-iodoamphetamine as a cerebral blood flow agent using emission tomography. *J. Nucl. Med.*, **31**, 1364–9.
- Greenberg, J. H., Hamar, J., Welsh, F. A., Harris, V. and Reivich, M. (1992). Effect of ischemia and reperfusion on the lumped constant of the [¹⁴C] deoxyglucose technique. *J. Cereb. Blood Flow Metab.*, **12**, 70–7.
- Grubb, R. L., Jr, Raichle, M. E., Phelps, M. E. and Ratcheson, R. A. (1975). Effects of increased intracranial pressure on cerebral blood volume, blood flow, and oxygen utilization in monkeys. *J. Neurosurg.*, **43**, 385–98.
- Grubb, R. L., Jr, Raichle, M. E., Higgins, C. S. and Eichling, J. O. (1978). Measurement of regional cerebral blood volume by emission tomography. *Ann. Neurol.*, **4**, 322–8.
- Hasselbalch, S. G., Madsen, P. L., Knudsen, G. M., Holm S. and Paulson O. B. (1998). Calculation of the FDG lumped constant by simultaneous measurements of global glucose and FDG metabolism in humans. *J. Cereb. Blood Flow Metab.*, **18**, 154–60.
- Hatazawa, J., Masatoshi, I., Matsuzawa, T., Ido, T. and Watanuki, S. (1988). Measurement of the ratio of cerebral oxygen consumption to glucose utilization by positron emission tomography: its consistency with the values determined by the Kety–Schmidt method in normal volunteers. *J. Cereb. Blood Flow Metab.*, **8**, 426–32.
- Heiss, W.-D. and Podreka, I. (1993). Role of PET and SPECT in the assessment of ischemic cerebrovascular disease. *Cerebrovasc. Brain Metabol. Rev.*, **5**, 235–63.
- Herscovitch, P. and Raichle, M. E. (1983). Effect of tissue heterogeneity on the measurement of cerebral blood flow with the equilibrium C¹⁵O₂ inhalation technique. *J. Cereb. Blood Flow Metab.*, **3**, 407–15.
- Herscovitch, P. and Raichle, M. E. (1985). What is the correct value for the brain–blood partition coefficient of water? *J. Cereb. Blood Flow Metab.*, **5**, 65–9.
- Herscovitch, P., Markham, J. and Raichle, M. E. (1983). Brain blood flow measured with intravenous H₂¹⁵O. I. Theory and error analysis. *J. Nucl. Med.*, **24**, 782–9.
- Herscovitch, P., Auchus, A., Gado, M., Chi, D. and Raichle, M. E. (1986). Correction of positron emission tomography data for cerebral atrophy. *J. Cereb. Blood Flow Metab.*, **6**, 120–4.
- Herscovitch, P., Raichle, M. E., Kilbourn, M. R. and Welch, M. J. (1987). Positron emission tomographic measurements of cerebral blood flow and permeability–surface area product of water using [¹⁵O]water and [¹¹C]butanol. *J. Cereb. Blood Flow Metab.*, **7**, 527–42.
- Hoffman, E. J. and Phelps, M. E. (1986). Positron emission tomography: principles and quantitation. In *Positron Emission Tomography and Autoradiography*, ed. M. E. Phelps, J. C. Mazziotta and H. R. Schelbert, pp. 237–86. New York: Raven Press.
- Hoffman, E. J., Huang, S.-C. and Phelps, M. E. (1979). Quantitation in positron emission computed tomography: 1. Effect of object size. *J. Comput. Assist. Tomogr.*, **3**, 299–308.
- Hoffman, E. J., Huang, S. C., Phelps, M. E. and Kuhl, D. E. (1981). Quantitation in positron emission computed tomography. 4. Effect of accidental coincidences. *J. Comput. Assist. Tomogr.*, **5**, 391–400.
- Holman, B. L. and Devous, M. S. (1992). Functional brain SPECT: the emergence of a powerful clinical method. *J. Nucl. Med.*, **33**, 1888–904.
- Holman, B. L., Carvalho, P. A., Zimmerman, R. E. et al. (1990). Brain perfusion SPECT using an annular single crystal camera: initial clinical experience. *J. Nucl. Med.*, **31**, 1456–61.
- Holman, B. L., Zimmerman, R. E., Johnson, K. A. et al. (1991). Computer-assisted superimposition of magnetic resonance and high-resolution technetium-99m-HMPAO and thallium-201 SPECT images of the brain. *J. Nucl. Med.*, **32**, 1478–84.
- Horwitz, B., Soncrant, T. T. and Haxby, J. V. (1992). Covariance analysis of functional interactions in the brain using metabolic and blood flow data. In *Advances in Metabolic Mapping Techniques for Brain Imaging of Behavioral and Learning Functions*, ed. F. Gonzalez-Lima, T. Finkenstaedt and H. Scheich, pp. 189–217. Dordrecht, the Netherlands: Kluwer.
- Huang, S.-C. and Phelps, M. E. (1986). Principles of tracer kinetic modeling in positron emission tomography and autoradiography. In *Positron Emission Tomography and Autoradiography*, ed. M. E. Phelps, J. C. Mazziotta and H. R. Schelbert, pp. 237–86. New York: Raven Press.

- Huang, S. C., Phelps, M. E., Hoffman, E. J., Sideris, K., Selin, C. J. and Kuhl, D. E. (1980). Non-invasive determination of local cerebral metabolic rate of glucose in man. *Am. J. Physiol.*, **238**, E69–82.
- Huang, S. C., Phelps, M. E., Hoffman, E. J. and Kuhl, D. E. (1981). Error sensitivity of fluorodeoxyglucose method for measurement of cerebral metabolic rate of glucose. *J. Cerebr. Blood Flow Metab.*, **1**, 391–401.
- Huda, W. and Scrimger, J. W. (1989). Irradiation of volunteers in nuclear medicine. *J. Nucl. Med.*, **30**, 260–4.
- Iida, H., Rhodes, C. G., de Silva, R. et al. (1992). Use of the left ventricular time–activity curve as a noninvasive input function in oxygen-15-water positron emission tomography. *J. Nucl. Med.*, **33**, 1669–77.
- Jacobs, A., Put, E., Ingels, M. and Bossuyt, A. (1994). Prospective evaluation of technetium-99m-HMPAO SPECT in mild and moderate traumatic brain injury. *J. Nucl. Med.*, **35**, 942–7.
- Jueptner, M. and Weiller, C. (1995). Does measurement of regional cerebral blood flow reflect synaptic activity – implications for PET and fMRI. [Review] *Neuroimage* **2**, 148–56.
- Juni, J. E. (1994). Taking brain SPECT seriously: reflections on recent clinical reports in the *Journal of Nuclear Medicine*. *J. Nucl. Med.*, **35**, 1891–5.
- Karp, J. S., Daube-Witherspoon, M. E., Hoffman, E. J. et al. (1991). Performance standards in positron emission tomography. *J. Nucl. Med.*, **32**, 2342–50.
- Kassis, A. I. (1992). The MIRD approach: remembering the limitations. *J. Nucl. Med.*, **33**, 781–2.
- Kety, S. S. (1951). The theory and applications of the exchange of inert gas at the lungs and tissues. *Pharmacol. Rev.*, **3**, 1–41.
- Kilbourn, M. (1991). Radiotracers for PET studies of neurotransmitter binding sites: design considerations. In *In Vivo Imaging of Neurotransmitter Functions in Brain, Heart and Tumors*, ed. D. E. Kuhl, pp. 47–65. Washington, DC: American College of Nuclear Physicians.
- Koepppe, R. A. and Hutchins, G. D. (1992). Instrumentation for positron emission tomography: tomographs and data processing and display systems. *Semin. Nucl. Med.*, **22**, 162–81.
- Koepppe, R. A., Holden, J. E. and Ip, W. R. (1985). Performance comparison of parameter estimation techniques for the quantitation of local cerebral blood flow by dynamic positron computed tomography. *J. Cerebr. Blood Flow Metab.*, **5**, 224–34.
- Koepppe, R. A., Holthoff, V. A., Frey, K. A., Kilbourn, M. R. and Kuhl, D. E. (1991). Compartmental analysis of [¹¹C]flumazenil kinetics for the estimation of ligand transport rate and receptor distribution using positron emission tomography. *J. Cerebr. Blood Flow Metab.*, **11**, 735–44.
- Kuhl, D. E., Alavi, A., Hoffman, E. J. et al. (1980). Local cerebral blood volume in head-injured patients: determination by emission computed tomography of ^{99m}Tc-labeled red cells. *J. Neurosurg.*, **52**, 309–20.
- Lammertsma, A. A., Jones, T., Frackowiak, R. S. J. and Lenzi, G.-L. (1981). A theoretical study of the steady-state model for measuring regional cerebral blood flow and oxygen utilization using oxygen-15. *J. Comput. Assist. Tomogr.*, **5**, 544–50.
- Lammertsma, A. A., Wise, R. J. S., Heather, J. D. et al. (1983). Correction for the presence of intravascular oxygen-15 in the steady-state technique for measuring regional oxygen extraction ratio in the brain. 2. Results in normal subjects and brain tumor and stroke patients. *J. Cerebr. Blood Flow Metab.*, **3**, 425–31.
- Lammertsma, A. A., Brooks, D. J., Beaney, R. P. et al. (1984). In vivo measurement of regional cerebral haematocrit using positron emission tomography. *J. Cerebr. Blood Flow Metab.*, **4**, 317–22.
- Lammertsma, A. A., Brooks, D. J., Frackowiak, R. S. J. et al. (1987). Measurement of glucose utilization with [¹⁸F]2-fluoro-2-deoxy-D-glucose: a comparison of different analytical methods. *J. Cerebr. Blood Flow Metab.*, **7**, 161–72.
- Landau, W. M., Freygang, W. H., Jr, Rowland, L. P., Sokoloff, L. and Kety, S. (1955). The local circulation of the living brain; values in the unanesthetized and anesthetized cat. *Trans. Am. Neurol. Assoc.*, **80**, 125–9.
- Laruelle, M., Baldwin, R. M., Rattner, Z. et al. (1994a). SPECT quantification of [¹²³I]iomazenil binding to benzodiazepine receptors in nonhuman primates. I. Kinetic modeling of single bolus experiments. *J. Cerebr. Blood Flow Metab.*, **14**, 439–52.
- Laruelle, M., van, Dyck, C., Abi, D. A. et al. (1994b). Compartmental modeling of iodine-123-iodobenzofuran binding to dopamine D₂ receptors in healthy subjects. *J. Nucl. Med.*, **35**, 743–54.
- Leenders, K. L., Perani, D., Lammertsma, A. A. et al. (1990). Cerebral blood flow, blood volume and oxygen utilization: normal values and effect of age. *Brain*, **113**, 27–47.
- Leniger-Follert, E. and Hossman, K.-A. (1979). Simultaneous measurements of microflow and evoked potentials in the somatomotor cortex of rat brain during specific sensory activation. *Pflugers Arch.*, **380**, 85–9.
- Lockwood, A. H. (1985). Invasiveness in studies of brain function by positron emission tomography. *J. Cerebr. Blood Flow Metab.*, **5**, 487–9.
- Loevinger, R., Budinger, T. F. and Watson, E. E. (1988). *MIRD Primer for Absorbed Dose Calculations*. New York: Society of Nuclear Medicine.
- Lou, H. C., Edvinsson, L. and MacKenzie, E. T. (1987). The concept of coupling blood flow to brain function: revision required? *Ann. Neurol.*, **22**, 289–97.
- Martin, W. R. W., Powers, W. J. and Raichle, M. E. (1987). Cerebral blood volume measured with inhaled C¹⁵O and positron emission tomography. *J. Cerebr. Blood Flow Metab.*, **7**, 421–6.
- Masdeu, J. C., Brass, L. M., Holman, B. L. and Kushner, M. J. (1994). Brain single-photon emission computed tomography. *Neurology*, **44**, 1970–7.
- Matthew, E., Andreason, P., Carson, R. E. et al. (1993). Reproducibility of resting cerebral blood-flow measurements with H₂¹⁵O positron emission tomography in humans. *J. Cerebr. Blood Flow Metab.*, **13**, 748–54.
- Mazziotta, J. C., Phelps, M. E., Plummer, D. and Kuhl, D. E. (1981). Quantitation in positron computed tomography. 5. Physical-anatomical effects. *J. Comput. Assist. Tomogr.*, **5**, 734–43.
- McIntosh, A. R., Grady, C. L., Ungerleider, L. G., Haxby, J. V., Rapoport, S. I. and Horwitz, B. (1994). Network analysis of cortical visual pathways mapped with PET. *J. Neurosci.*, **14**, 655–66.
- Meltzer, C. C., Zubieta, J. K., Links, J. M., Brakeman, P., Stumpf, M. J. and Frost, J. J. (1996). MR-based correction of brain PET

- measurements for heterogeneous gray-matter radioactivity distribution. *J. Cereb. Blood Flow Metab.*, **16**, 650–8.
- Minoshima, S., Berger, K. L., Lee, K. S. and Mintun, M. A. (1992). An automated method for rotational correction and centering of three-dimensional functional brain images. *J. Nucl. Med.*, **33**, 1579–85.
- Mintun, M. A., Raichle, M. E., Martin, W. R. W. and Herscovitch, P. (1984). Brain oxygen utilization measured with O-15 radiotracers and positron emission tomography. *J. Nucl. Med.*, **25**, 177–87.
- Murase, K., Tanada, S., Fujita, H., Sakaki, S. and Hamamoto, K. (1992). Kinetic behavior of technetium-99m-HMPAO in human brain and quantification of cerebral blood flow using dynamic SPECT. *J. Nucl. Med.*, **33**, 135–43.
- Muzik, O., Chugani, D. C., Shen, C. and Chugani, H. T. (1998). Noninvasive imaging of serotonin synthesis rate using PET and α -methyltryptophan in autistic children. In *Quantitative Functional Brain Imaging with Positron Emission Tomography*, ed. R. E. Carson, M. E. Daube-Witherspoon and P. Herscovitch, pp. 201–6. San Diego, CA: Academic Press.
- Nakai, H., Yamamoto, Y. L., Diksic, M. et al. (1987). Time-dependent changes of lumped and rate constants in the deoxyglucose method in experimental cerebral ischemia. *J. Cereb. Blood Flow Metab.*, **7**, 640–8.
- Obrist, W. D., Langfitt, T. W., Jaggi, J., Cruz, J. and Gennarelli, T. A. (1984). Cerebral blood flow and metabolism in comatose patients with acute head injury. *J. Neurosurg.*, **61**, 241–53.
- Ohta, S., Meyer, E., Thompson, C. J. and Gjedde, A. (1992). Oxygen consumption of the living human brain measured after a single inhalation of positron emitting oxygen. *J. Cereb. Blood Flow Metab.*, **12**, 179–92.
- Pelizzari, C. A., Chen, G. T. Y., Spelbring, D. R., Weichselbaum, R. R. and Chen, C.-T. (1989). Accurate three-dimensional registration of CT, PET, and/or MR images of the brain. *J. Comput. Assist. Tomogr.*, **13**, 20–6.
- Perlman, J. M. and Altman, D. I. (1992). Symmetric cerebral blood flow in newborns who have undergone successful extracorporeal membrane oxygenation. *Pediatrics*, **89**, 235–9.
- Perlmutter, J. S., Powers, W. J., Herscovitch, P., Fox, P. T. and Raichle, M. E. (1987). Regional asymmetries of cerebral blood flow, blood volume, oxygen utilization and extraction in normal subjects. *J. Cereb. Blood Flow Metab.*, **7**, 64–7.
- Phelps, M. E. and Hoffman, E. J. (1976). Resolution limit of positron cameras. *J. Nucl. Med.*, **17**, 757–8.
- Phelps, M. E., Huang, S. C., Hoffman, E. J., Selin, C., Sokoloff, L. and Kuhl, D. E. (1979). Tomographic measurement of local cerebral glucose metabolic rate in humans with (F-18) 2-fluoro-2-deoxy-D-glucose: validation of method. *Ann. Neurol.*, **6**, 371–88.
- Powers, W. J. (1988). Positron emission tomography in the evaluation of cerebrovascular disease: clinical applications? In *Clinical Neuroimaging*, ed. W. H. Theodore, pp. 49–74. New York: Alan R. Liss.
- Powers, W. J. (1991). Cerebral hemodynamics in ischemic cerebrovascular disease. *Ann. Neurol.*, **29**, 231–40.
- Powers, W. J., Berg, L., Perlmutter, J. S. and Raichle, M. E. (1991). Technology assessment revisited: does positron emission tomography have proven clinical efficacy? *Neurology*, **41**, 1339–40.
- Powers, W. J., Rosenbaum, J. L., Dence, C. S., Markham, J. and Videen, T. O. (1998). Cerebral glucose transport and metabolism in preterm human infants. *J. Cereb. Blood Flow Metab.*, **18**, 632–8.
- Raichle, M. E. (1987). Circulatory and metabolic correlates of brain function in normal humans. In *Handbook of Physiology: The Nervous System*, ed. V. B. Mountcastle and F. Plum, pp. 643–74. Bethesda, MD: American Physiological Society.
- Raichle, M. E. (1991). The metabolic requirements of functional activity in human brain: a positron emission tomography study. In *Fuel Homeostasis and the Nervous System*, ed. M. Vranic, S. Efenic and C. H. Hollenberg, pp. 1–4. New York: Plenum.
- Raichle, M. E., Martin, W. R. W., Herscovitch, P., Mintun, M. A. and Markham, J. (1983). Brain blood flow measured with intravenous $H_2^{15}O$. II. Implementation and validation. *J. Nucl. Med.*, **24**, 790–8.
- Rajapakse, J. C., Giedd, J. N., Rumsey, J. M., Vaituzis, A. C., Hamburger, S. D. and Rapoport, J. L. (1996). Regional MRI measurements of the corpus callosum: a methodological and developmental study. *Brain Dev.*, **18**, 379–88.
- Reivich, M., Kuhl, D., Wolf, A. et al. (1979). The [^{18}F]fluorodeoxyglucose method for the measurement of local cerebral glucose utilization in man. *Circ. Res.*, **44**, 127–37.
- Reivich, M., Alavi, A., Wolf, A. et al. (1985). Glucose metabolic rate kinetic model parameter determination in humans: the lumped constants and rate constants for [^{18}F]fluorodeoxyglucose and [^{14}C]deoxyglucose. *J. Cereb. Blood Flow Metab.*, **5**, 179–92.
- Sasaki, H., Kanno, I., Murakami, M., Shishido, F. and Uemera, K. (1986). Tomographic mapping of kinetic rate constants in the fluorodeoxyglucose model using dynamic positron emission tomography. *J. Cereb. Blood Flow Metab.*, **6**, 447–54.
- Seibyl, J. P., Laruelle, M., van Dyck, C. H. et al. (1996). Reproducibility of iodine-123- β -CIT SPECT brain measurement of dopamine transporters. *J. Nucl. Med.*, **37**, 222–8.
- Sokoloff, L. (1961). Local cerebral circulation at rest and during altered cerebral activity induced by anesthesia or visual stimulation. In *Regional Neurochemistry*, ed. S. S. Kety and J. Elkes, pp. 107–17. New York: Pergamon Press.
- Sokoloff, L. (1981). Relationships among local functional activity, energy metabolism, and blood flow in the central nervous system. *FASEB J.*, **40**, 2311–16.
- Sokoloff, L. (1985). Basic principles in imaging of cerebral metabolic rates. In *Brain Imaging and Brain Function*, ed. L. Sokoloff, pp. 21–49. New York: Raven Press.
- Sokoloff, L., Reivich, M., Kennedy, C. et al. (1977). The [^{14}C]deoxyglucose method for the measurement of local cerebral glucose utilization; theory, procedure, and normal values in the conscious and anesthetized albino rat. *J. Neurochem.*, **28**, 897–916.
- Sorenson, J. A. and Phelps, M. E. (1987). *Physics in Nuclear Medicine*. Orlando, FL: Grune and Stratton.
- Spence, A. M., Graham, M. M., Muzi, M. et al. (1990). Deoxyglucose lumped constant estimated in a transplanted rat astrocytic glioma by the hexose utilization index. *J. Cereb. Blood Flow Metab.*, **10**, 190–8.
- Spinks, T. J., Jones, T., Bailey, D. L. et al. (1992). Physical performance of a positron tomograph for brain imaging with retractable septa. *Phys. Med. Biol.*, **37**, 1637–55.

- Stapleton, S. J., Caldwell, C. B., Leonhardt, C. L., Ehrlich, L. E., Black, S. E. and Yaffe, M. J. (1994). Determination of thresholds for detection of cerebellar blood flow deficits in brain SPECT images. *J. Nucl. Med.*, **35**, 1547–55.
- Strother, S. C., Kanno, I. and Rottenberg, D. A. (1995). Commentary and opinion. 1. Principal component analysis, variance partitioning, and functional connectivity. *J. Cereb. Blood Flow Metab.*, **15**, 353–60.
- Subramanyam, R., Alpert, N. M., Hoop, B., Jr, Brownell, G. L. and Taveras, J. M. (1978). A model for regional cerebral oxygen distribution during continuous inhalation of $^{15}\text{O}_2$, C^{15}O , and C^{15}O_2 . *J. Nucl. Med.*, **19**, 13–53.
- Ter-Pogossian, M. M. (1992). The origins of positron emission tomography. *Semin. Nucl. Med.*, **22**, 140–9.
- Ter-Pogossian, M. M., Phelps, M. E., Hoffman, E. J. and Mullani, N. A. (1975). A positron-emission transaxial tomograph for nuclear imaging (PETT). *Radiology*, **114**, 89–98.
- Toga, A. W. and Collins, R. C. (1981). Metabolic response of optic centers to visual stimuli in the albino rat: anatomical and physiological considerations. *J. Comp. Neurol.*, **199**, 443–64.
- Tyler, J. L., Strother, S. C., Zatorre, R. J. et al. (1988). Stability of regional cerebral glucose metabolism in the normal brain measured by positron emission tomography. *J. Nucl. Med.*, **29**, 631–42.
- van Bogaert, P., Wikler, D., Damhaut, P., Szliwowska, H. B. and Goldman, S. (1998). Regional changes in glucose metabolism during brain development from the age of 6 years. *Neuroimage*, **8**, 62–8.
- van Heertum, R. L., Miller, S. H. and Mosesson, R. E. (1993). SPECT brain imaging in neurologic disease. *Radiol. Clin. North Am.*, **31**, 881–907.
- Veatch, R. M. (1982). The ethics of research involving radiation. *IRB: Rev. Hum. Subjects Res.*, **4**, 3–5.
- Videen, T. O., Perlmutter, J. S., Herscovitch, P. and Raichle, M. E. (1987). Brain blood volume, flow, and oxygen utilization measured with ^{15}O radiotracers and positron emission tomography: revised metabolic computations. *J. Cereb. Blood Flow Metab.*, **7**, 513–16.
- Videen, T. O., Perlmutter, J. S., Mintun, M. A. and Raichle, M. E. (1988). Regional correction of positron emission tomography data for the effects of cerebral atrophy. *J. Cereb. Blood Flow Metab.*, **8**, 662–70.
- Volkow, N. and Fowler, J. S. (1992). Neuropsychiatric disorders: investigation of schizophrenia and substance abuse. *Semin. Nucl. Med.*, **22**, 254–67.
- Volpe, J. J., Herscovitch, P., Perlman, J. M. and Raichle, M. E. (1983). Positron emission tomography in the newborn: Extensive impairment of regional cerebral blood flow with intraventricular hemorrhage and hemorrhagic intracerebral involvement. *Pediatrics*, **72**, 589–601.
- Wang, B., Thompson, C. J., Tremblay, H., Reutens, D., Jolly, D. and Meyer, E. (1998). Measurement of the evoked vascular response (EVR) to cerebral activation due to vibro-tactile stimulation using gated C-11-CO PET acquisition. *IEEE Trans. Nucl. Sci.*, **45**, 1111–16.
- Wang, G.-J., Volkow, N. D., Wolf, A. P., Brodie, J. D. and Hitzeman, R. J. (1994). Intersubject variability of brain glucose metabolic measurements in young normal males. *J. Nucl. Med.*, **35**, 1457–66.
- Warner, D. S., Kassell, N. F. and Boarini, D. J. (1987). Microsphere cerebral blood flow determination. In *Cerebral Blood Flow: Physiologic and Clinical Aspects*, ed. J. H. Wood, pp. 288–98. New York: McGraw-Hill.
- Weinberg, I. N., Huang, S. C., Hoffman, E. J. et al. (1988). Validation of PET-acquired input functions for cardiac studies. *J. Nucl. Med.*, **29**, 241–7.
- Wienhard, K., Pawlik, G., Herholz, K., Wagner, R. and Heiss, W.-D. (1985). Estimation of local cerebral glucose utilization by positron emission tomography of ^{18}F 2-fluoro-2-deoxy-D-glucose: a critical appraisal of optimization procedures. *J. Cereb. Blood Flow Metab.*, **5**, 115–25.
- Wienhard, K., Dahlbom, M., Eriksson, L. et al. (1994). The ECAT EXACT HR: performance of a new high resolution positron scanner. *J. Comput. Assist. Tomogr.*, **18**, 110–18.
- Wilson, J. T. L. and Wyper, D. (1992). Neuroimaging and neurological functioning following closed head injury: CT, MRI, and SPECT. *J. Head Trauma Rehab.*, **7**, 29–39.
- Wilson, M. W. and Mountz, J. M. (1989). A reference system for neuroanatomical localization on functional reconstructed cerebral images. *J. Comput. Assist. Tomogr.*, **13**, 174–8.
- Wolf, A. P. and Schlyer, D. J. (1993). Accelerators for positron emission tomography. In *Nuclear Imaging in Drug Discovery, Development, and Approval*, ed. D. H. Burns, R. E. Gibson, R. F. Dannals and P. K. S. Siegl, pp. 33–54. Boston: Birkhäuser.
- Woods, R. P., Mazziotta, J. C. and Cherry, S. R. (1993). MRI-PET registration with automated algorithm. *J. Comput. Assist. Tomogr.*, **17**, 536–46.
- Wyper, D. J. (1993). Functional neuroimaging with single photon emission computed tomography (SPECT). *Cerebrovasc. Brain Metabo. Rev.*, **5**, 199–217.
- Yarowsky, P. J. and Ingvar, D. H. (1981). Neuronal activity and energy metabolism. *Fed. Proc.*, **40**, 2353–62.
- Yarowsky, P., Kadakara, M. and Sokoloff, L. (1983). Frequency-dependent activation of glucose utilization in the superior cervical ganglion by electrical stimulation of cervical sympathetic trunk. *Proc. Nat. Acad. Sci. USA*, **80**, 4179–83.
- Zametkin, A. J., Liebenauer, L. L., Fitzgerald, G. A. et al. (1993). Brain metabolism in teenagers with attention deficit hyperactivity disorder. *Arch. Gen. Psychiatry*, **50**, 333–40.